

Aerosol size distribution and radiative forcing response to anthropogenically driven historical changes in biogenic secondary organic aerosol formation

S. D. D'Andrea¹, J. C. Acosta Navarro², S. C. Farina¹, C. E. Scott³, A. Rap³, D. K. Farmer⁴, D. V. Spracklen³, I. Riipinen^{2,5}, J. R. Pierce¹

[1]{Department of Atmospheric Science, Colorado State University, Fort Collins, CO, USA}

[2]{Department of Applied Environmental Science and Bert Bolin Centre for Climate Research, Stockholm University, Stockholm, Sweden}

[3]{School of Earth and Environment, University of Leeds, Leeds, United Kingdom}

[4]{Department of Chemistry, Colorado State University, Fort Collins, CO, USA}

[5]{Center for Atmospheric Particle Studies, Carnegie Mellon University, Pittsburgh, PA, USA}

Correspondence to: sdandrea@atmos.colostate.edu

Abstract

Emissions of biogenic volatile organic compounds (BVOC) have changed in the past millennium due to changes in land use, temperature and CO₂ concentrations. Recent reconstructions of BVOC emissions predicted that global isoprene emissions have decreased, while monoterpene and sesquiterpene emissions have increased; however, all three show regional variability due to competition between the various influencing factors.

In this work, we use two modeled estimates of BVOC emissions from the years 1000 to 2000 to test the effect of anthropogenic changes to BVOC emissions on SOA formation, global aerosol size distributions, and radiative effects using the GEOS-Chem-TOMAS global aerosol microphysics model. With anthropogenic emissions (e.g. SO₂, NO_x, primary aerosols) turned off and BVOC emissions changed from year 1000 to year 2000 values, decreases in the number concentration of particles of size $D_p > 80$ nm (N80) of >25% in year 2000 relative to year 1000 were predicted in regions with extensive land-use changes since year 1000 which led to regional increases in the combined aerosol radiative effect (direct and indirect) of >0.5 W m⁻² in these regions. We test the sensitivity of our results to BVOC emissions inventory, SOA yields and the presence of anthropogenic emissions; however, the qualitative response of the model to

1 historic BVOC changes remains the same in all cases. Accounting for these uncertainties, we
2 estimate millennial changes in BVOC emissions cause a global mean direct effect of between
3 +0.022 and +0.163 W m⁻² and the global mean cloud-albedo aerosol indirect effect of between -
4 0.008 and -0.056 W m⁻². This change in aerosols, and the associated radiative forcing, could be
5 a largely overlooked and important anthropogenic aerosol effect on regional climates.

6 7 **1 Introduction**

8 Biogenic volatile organic compounds (BVOCs) play an important role in tropospheric chemistry
9 and pollution by reacting with the hydroxyl radical (OH), nitrate radical (NO₃), and ozone (O₃)
10 (Chung et al., 2002). BVOCs are also important precursors for O₃ (Chameides et al., 1998) and
11 secondary organic aerosol (SOA) formation (Kanakidou et al., 2005). Recent studies on
12 historical emissions of BVOCs have shown that BVOC emissions have been affected by
13 anthropogenic influences over the past millennium (Kaplan et al., 2011; Tanaka et al., 2012;
14 Pacifico et al., 2012; Unger, 2013; Acosta Navarro et al., 2014). Changes in land use,
15 temperature, and carbon dioxide (CO₂) concentrations have all had significant impacts on the
16 emissions of BVOCs.

17 Acosta Navarro et al. (2014) predicted that globally averaged isoprene emissions have
18 decreased over the past millennium mainly due to land-use changes, which involved the
19 conversion of high isoprene-emitting natural shrubs and broadleaf trees to low emitting crop and
20 grazing land. They also predicted that globally averaged monoterpene and sesquiterpene
21 emissions have increased over the past millennium due mainly to global increases in
22 temperature (the monoterpene- and sesquiterpene-emitting vegetation has not decreased from
23 land-use changes to the same degree as the isoprene-emitting vegetation). However, all three
24 BVOC classes show both increases and decreases in various regions due to competing factors
25 such as land-use change, increases in CO₂ concentrations and temperature change. The most
26 dominant cause of BVOC emission changes has been from anthropogenic factors (e.g. change
27 in land cover and CO₂ effects), where land-use change has had the most dramatic impact by
28 decreasing the isoprene emissions. These changes in BVOC emissions can have important
29 implications on the formation rate of low-volatility SOA, which is essential for particle growth to
30 sizes large enough to affect climate (Riipinen et al., 2011, 2012; Paasonen et al., 2013; Liao et
31 al., 2014).

32 The Earth's radiation balance is directly affected by aerosol particles by absorption and
33 scattering of solar radiation (Rosenfeld et al., 2008; Clement et al., 2009) as well as indirectly
34 affected by aerosols by alteration of cloud properties and lifetimes (Charlson et al., 1992). The

1 uncertainty associated with aerosol radiative forcing, particularly the aerosol indirect effect, is a
2 large source of uncertainty in global climate models (Solomon et al., 2007). Recent studies
3 suggest that this uncertainty is largely due to incomplete knowledge on different natural
4 contributions to atmospheric aerosol loadings (Carslaw et al., 2013). The influence of aerosols
5 on cloud droplet number concentration (CDNC) is driven by the number concentration of cloud
6 condensation nuclei (CCN), or the particles on which cloud droplets form. The number
7 concentration of CCN is highly dependent on the aerosol size distribution (Dusek et al., 2006;
8 McFiggans et al., 2006; Petters and Kreidenweis, 2007; Pierce and Adams, 2007), therefore the
9 size-dependent number of all sizes of particles must be accurately represented to simulate CCN
10 number concentrations correctly.

11 The two sources of aerosol number to the atmosphere are by primary emissions (Putaud
12 et al., 2004; Stanier et al., 2004) and by the formation of new particles (diameter ~1 nm) via
13 nucleation (Kulmala et al., 2004). In order for freshly nucleated particles or emitted
14 nanoparticles with diameters less than CCN sizes (30-100 nm) to influence atmospheric CCN
15 number concentrations, they must undergo condensational growth (Pierce and Adams, 2007;
16 Vehkamäki and Riipinen, 2012). However, the survival probability of nanoparticles depends on
17 the competition between condensational growth and coagulative scavenging with pre-existing
18 aerosol (Kerminen and Kulmala, 2002; Pierce and Adams, 2007; Kuang et al., 2009; Westervelt
19 et al., 2013).

20 The growth of particles to CCN sizes due to condensation of sulfuric acid is well known
21 (Sipilä et al., 2010); however, the condensation of low-volatility organic aerosols (OA) have also
22 recently been shown to play a substantial role in particle growth (Kerminen et al., 2012; Riipinen
23 et al., 2011, 2012; Carslaw et al., 2010; Makkonen et al., 2012). Measurements of the
24 submicron particle composition throughout the continental boundary layer show that 20 – 90%
25 of the submicron particulate mass is OA (Jimenez et al., 2009). OA enters the atmosphere
26 through biogenic emissions as well as by anthropogenic emission sources such as vehicles or
27 residential heating (Hallquist et al., 2009). Volatile organic compounds (VOCs), biogenic volatile
28 organic compounds (BVOCs), and intermediate volatility organic compounds have been shown
29 to be precursors for SOA (Donahue et al., 2011; Hallquist et al., 2009). SOA formation occurs
30 when gas phase, particle-phase, and cloud-phase chemical processes involving VOCs form
31 products with low enough volatility to remain in the condensed phase (Hallquist et al., 2009; Lim
32 et al., 2010). Additionally, in regions where there is mixing of anthropogenic and biogenic
33 species, anthropogenic species may enhance SOA formation from BVOCs (Carleton et al.,
34 2010; Spracklen et al., 2011a, de Gouw et al., 2005). Regardless of the formation mechanism,

1 adding SOA mass to pre-existing aerosol causes a net condensational flux to the aerosol
2 phase. This increased condensational flux can enhance the growth of ultrafine aerosols to
3 climate-relevant sizes (Pierce et al., 2011; Riipinen et al., 2011, D’Andrea et al., 2013).
4 Therefore, BVOC emissions have a significant impact on SOA formation, CCN number
5 concentrations, and ultimately climate.

6 In this paper, we test the influence of anthropogenic changes in BVOC emissions on
7 SOA formation, global aerosol size distributions, and CCN by using these modeled estimates of
8 the dominant BVOC classes’ emissions from the years 1000 to 2000. The year 1000 was
9 chosen (as opposed to the years 1750 or 1800) to not only capture pre-industrial conditions, but
10 also account for changes in isoprene emissions prior to 1750 through human-induced land-use
11 changes. Furthermore, we quantify the net radiative forcing associated with these
12 anthropogenic BVOC changes. Previous studies have investigated the impacts of land-use
13 change on aerosols and radiative forcing (Heald et al., 2008; Wu et al., 2012; Ward et al., 2014),
14 however this study focuses uniquely on the combination of historical perspective,
15 comprehensive consideration of different BVOC species, and detailed aerosol microphysics
16 (thus focusing on the aerosol number concentrations and size distributions). We do not take
17 into account the potential effects of changing anthropogenic pollution on the yields of biogenic
18 SOA from BVOCs because of the large uncertainties in these enhancements, but we discuss
19 the implications of these changes. In the following section, we summarize the global millennial
20 changes in biogenic emissions from Acosta Navarro et al. (2014). Section 3 describes the
21 model used in this study and the methods used for formation of SOA from the biogenic
22 terpenoid emissions. Section 4 describes the results, highlighting the global changes in particle
23 size distributions due to the millennial changes in BVOC emissions and the climatic implications
24 associated with these changes.

25
26

27 **2 Overview of predicted BVOC emissions changes**

28 Acosta Navarro et al. (2014) used the Model of Emissions and Gases and Aerosols from Nature
29 (MEGAN) (Guenther et al., 2006) and the Lund-Potsdam-Jena General Ecosystem Generator
30 (LPJ-GUESS) (Smith et al., 2001; Sitch et al., 2003) to reconstruct BVOC emissions from the
31 year 1000 to the year 2000. This is described in detail by Acosta Navarro et al. (2014), but will
32 be summarized here. For this study, we refer to the decadal-averaged BVOC emissions using
33 MEGAN from 1000-1010 and from 1980-1990 as years 1000 and 2000, respectively, for
34 simplicity. We refer to the annual-averaged BVOC emissions using LPJ-GUESS from years

1 1000 and 2000 as years 1000 and 2000, respectively. Because our LPJ-GUESS emissions are
2 from one single year at 1000 and 2000, these data may be susceptible to some regional biases
3 due to not capturing interannual variability.

4 The MEGAN reconstruction includes all three BVOC classes, whereas the LPJ-GUESS
5 reconstruction includes only isoprene and monoterpenes. MEGAN and LPJ-GUESS were run
6 in a series of simulations testing sensitivities to variables (such as plant functional type, leaf
7 area index, soil water content, annual CO₂ concentrations, land-use cover, and anthropogenic
8 vegetation types such as crops and pastures), and millennial terpenoid BVOC emission
9 inventories were created (Acosta Navarro et al., 2014). The main driving factors behind the
10 changes are not always the same (for details see Acosta Navarro et al. (2014)).

11 The terpenoid BVOC emissions in Acosta Navarro et al. (2014) are sensitive to
12 variations in meteorological conditions and land-use changes, but are also sensitive to the
13 empirical standard emission factors used in the developing of the inventory. Plant emission
14 factors of the three BVOCs were averaged over wide plant families in order to make the model
15 computationally feasible. Therefore, the changes in isoprene, monoterpenes and
16 sesquiterpenes in the reconstruction are indicators of the response of the three BVOCs to
17 external stresses and land-use change, rather than exact emission estimates. Also, changing
18 the resolution of the emissions inventory from the original resolution to a coarser resolution may
19 inherently have uncertainties.

20 Isoprene has the highest predicted emission rates of the BVOCs investigated in this
21 study with emissions averaged over the time period 1000-1990 greater than 50 mg m⁻² day⁻¹
22 using MEGAN and greater than 30 mg m⁻² day⁻¹ averaged over the period 1000-2000 using
23 LPJ-GUESS over tropical rainforests (Acosta Navarro et al., 2014). These emissions are
24 roughly a factor of 100 lower over mid-latitude forests. Isoprene emissions are dominant in
25 tropical and sub-tropical regions but much lower in boreal regions. Predicted absolute changes
26 in the spatial distribution of mean isoprene emissions from 1000 to 2000 using MEGAN and
27 LPJ-GUESS are shown in Figure 1a and 1b respectively. Globally averaged, predicted
28 isoprene emissions over this period decrease by 21% in MEGAN and 23% in LPJ-GUESS, and
29 these decreases are due predominantly to cropland expansion and CO₂ concentration effects
30 (Acosta Navarro et al., 2014). The changes in land-use due to natural high isoprene-emitting
31 broadleaf trees and shrubs being converted to low isoprene emitting crops and grasses, such as
32 in plantations and pastures, have directly decreased isoprene emissions regionally in both
33 reconstructions. The tropical and sub-tropical regions with high isoprene emissions are the
34 regions with the largest absolute changes in emission over this time period. There is some

1 evidence for decreases in isoprene emissions with increasing CO₂ concentrations, although the
2 related mechanisms are not well understood (Peñuelas et al., 2010). The effects are included in
3 MEGAN and LPJ-GUESS, so both of the models applied by Acosta Navarro et al. (2014)
4 suggest that increasing CO₂ concentrations in the present-day atmosphere also contribute to
5 the decrease in isoprene emissions. However, isoprene emissions in some regions where the
6 natural vegetation has remained unaltered or increased over the past millennium have
7 increased by greater than 50% in both reconstructions due to the increase in surface air
8 temperature (Acosta Navarro et al., 2014).

9 Along with changes in isoprene emissions over the past millennium, predicted
10 monoterpene emissions also change, but due to different environmental and anthropogenic
11 influences. Mean predicted emissions of monoterpenes over the period 1000-2000 are roughly
12 an order of magnitude lower than predicted isoprene emissions, but are still greater than 5 mg
13 m⁻² day⁻¹ and 0.8 mg m⁻² day⁻¹ in tropical and sub-tropical forests in the MEGAN and LPJ-
14 GUESS reconstructions respectively (Acosta Navarro et al., 2014). Predicted absolute changes
15 in the spatial distribution of mean monoterpene emissions from 1000 to 2000 using MEGAN and
16 LPJ-GUESS are shown in Figure 1c and 1d respectively. Globally averaged, predicted
17 monoterpene emissions over this period increase by 3% in MEGAN and 0% in LPJ-GUESS.
18 However, in many regions there is an increase in predicted monoterpene emissions of
19 approximately 0.5 mg m⁻² day⁻¹. These increases are due predominantly to the development of
20 agriculture in regions where monoterpene emitting vegetation was previously scarce (Acosta
21 Navarro et al., 2014). There are significant regions of decreasing monoterpene emissions in
22 both reconstructions (blue regions) due to strong deforestation and a replacement of natural
23 vegetation with low monoterpene-emitting species (Acosta Navarro et al., 2014). It is worthwhile
24 to note that the effect of CO₂ concentrations on monoterpene emissions is still under debate,
25 and was not included in the simulations by Acosta Navarro et al. (2014) applied here. We also
26 note that the temperature response of BVOC emissions used to predict long-term changes is
27 derived from short-term measurements, and may not accurately reflect adaptive behavior of
28 plants grown under changing environmental conditions.

29 Similar to changes in predicted monoterpene emissions over the past millennium,
30 sesquiterpene emissions have also been predicted to increase regionally, however remain
31 approximately constant globally. Mean predicted emissions of sesquiterpenes over the period
32 1000-2000 are spatially distributed similar to that of monoterpene emissions and are an order of
33 magnitude lower than predicted monoterpene emissions, and two orders of magnitude lower
34 than predicted isoprene emissions. Figure 1e shows the absolute change in predicted

1 sesquiterpene emissions from 1000 to 2000 using MEGAN. Following the same trend as
2 predicted monoterpenes, the globally averaged change in predicted sesquiterpene emissions
3 over this period increase by approximately 1%. The causes of the changes in predicted
4 sesquiterpene emissions are analogous to the changes in predicted monoterpene emissions.
5 The changes are predominantly due to development of agriculture in regions where
6 sesquiterpene emitting vegetation was previously limited (Acosta Navarro et al., 2014).

7

8 **3 Methods**

9 We use a global chemical transport model with online aerosol microphysics to test the sensitivity
10 of the simulated aerosol size distributions to changes in BVOC emissions from the years 1000
11 to 2000, and calculate the associated radiative forcing.

12

13 **3.1 GEOS-Chem-TOMAS Model Description**

14 We use the global chemical-transport model, GEOS-Chem (www.geos-chem.org), combined
15 with the online aerosol microphysics module, TOMAS (GEOS-Chem-TOMAS) to test the
16 sensitivity of global aerosol size distributions to changes in BVOC emissions. GEOS-Chem-
17 TOMAS in this study uses GEOS-Chem v9.01.02 with 4°x5° horizontal resolution, 47 vertical
18 layers from the surface to 0.01 hPa with meteorological inputs from the GEOS5 reanalysis
19 (<http://gmao.gsfc.nasa.gov>). TOMAS in this work simulates the aerosol size distribution using
20 15 size sections ranging from 3 nm to 10 μm (Lee and Adams, 2011). Nucleation rates in all
21 simulations were predicted by ternary homogeneous nucleation of sulfuric acid, ammonia, and
22 water based on the parameterization of Napari et al. (2002) scaled globally by a constant factor
23 of 10⁻⁵ which has been shown to predict nucleation rates closer to measurements than other
24 commonly used nucleation schemes (Jung et al., 2010; Westervelt et al., 2013). All emissions
25 except terpenoid biogenic emissions (monoterpenes, isoprene, and sesquiterpenes) in GEOS-
26 Chem are described in van Donkelaar et al. (2008). The three dominant BVOC classes
27 (monoterpenes, isoprene, and sesquiterpenes) are included in GEOS-Chem using modeled
28 reconstructions as provided by Acosta Navarro et al. (2014). The emissions from Acosta
29 Navarro et al. (2014) override biogenic emissions previously input from a different version of
30 MEGAN (Guenther et al., 2006) in the standard version of GEOS-Chem for SOA production
31 only and do not influence the gas-phase chemistry in GEOS-Chem-TOMAS. We are not
32 considering this feedback; however, we will discuss the implications in section 4.4.

33 Traditionally, SOA in GEOS-Chem-TOMAS is formed only from terrestrial biogenic
34 sources, with the biogenic source being a fixed yield of 10% of the monoterpene emissions.

1 However, isoprene and sesquiterpenes also serve as SOA precursors (Hoffmann et al., 1997;
2 Griffin et al., 1999a; Kroll et al., 2006). In this study, we form SOA from isoprene,
3 monoterpenes and sesquiterpenes with fixed yields of 3%, 10% and 20%, respectively, based
4 on estimations summarized in Pye et al. (2010). Dynamic SOA yields through partitioning
5 theory are computationally expensive to couple with aerosol microphysics schemes, and they
6 tend to underpredict ultrafine particle growth when lab-based volatility distributions are used
7 (Pierce et al., 2011), and thus are not used here. However, we test the sensitivity to these
8 yields. The yields used in this study are on the low end of mean yield estimates; however, we
9 test the sensitivity of SOA formation and CCN number concentrations to upper bounds on these
10 yields (10%, 20%, and 40%, respectively) (Pye et al., 2010) (see Table 1 for total biogenic SOA
11 formation rates for each simulation). Biogenic SOA formation, particularly from isoprene, has
12 been shown in chamber studies and ambient measurements to have dependencies on NO_x
13 concentrations (NO_x=NO+NO₂) (Kroll et al., 2006; Kroll and Seinfeld, 2008; Carlton et al., 2009;
14 Xu et al., 2014). SOA yield from isoprene oxidation can reach in excess of 4% under low-NO_x
15 conditions (Kroll et al., 2006) at atmospherically relevant organic mass concentrations (Carlton
16 et al., 2009). Kroll et al. (2006) also found in chamber studies that SOA yields from isoprene
17 oxidation can reach in excess of 5% at NO_x concentrations of approximately 100 ppb. Over the
18 past millenium, there have been increases in agriculture, anthropogenic biomass burning and
19 industrial activity leading to enhanced NO_x emissions (Benkovitz et al., 1996), which potentially
20 impact SOA yields. More sophisticated SOA formation mechanisms that account for NO_x-
21 dependent yields might improve model representation; however, maximum NO_x concentrations
22 in GEOS-Chem-TOMAS are approximately an order of magnitude lower than the concentrations
23 used in the chamber study by Kroll et al. (2006) (Lamsal et al., 2008) and therefore fall well
24 below NO_x concentrations high enough to significantly alter SOA formation rates. We note that
25 while high absolute concentrations of any species may call into question the atmospheric
26 relevance of chamber experiments, the NO:HO₂ ratio within a chamber is an equally critical
27 parameter for describing the chemical regime of SOA formation. Therefore, for this study,
28 biogenic SOA in GEOS-Chem-TOMAS is formed via fixed yields of isoprene, monoterpenes,
29 and sesquiterpenes, and has no dependency on NO_x concentrations. The change in emissions
30 of isoprene, monoterpenes, and sesquiterpenes from the MEGAN and LPJ-GUESS
31 reconstructions solely affects SOA formation, and does not influence the oxidation fields in
32 GEOS-Chem-TOMAS. Therefore, there may be missing feedback mechanisms on key
33 atmospheric oxidants.

1 In this study, particles are assumed to undergo kinetic, gas-phase-diffusion-limited
2 growth with condensation of SOA proportional to the Fuchs-corrected aerosol surface area.
3 This assumption was found to best reproduce aerosol size distribution in two recent studies
4 (Riipinen et al., 2011; D'Andrea et al., 2013). This kinetic condensation of SOA assumes that
5 the SOA is non-volatile (or similar to low-volatility SOA with average saturation vapor pressure,
6 C^* , of less than approximately $10^{-3} \mu\text{g m}^{-3}$) (Pierce et al., 2011, Ehn et al., 2014). Also, as
7 described in D'Andrea et al. (2013), an additional 100 Tg yr^{-1} of SOA correlated with
8 anthropogenic carbon monoxide emissions is required to match present-day measurements.
9 D'Andrea et al. (2013) evaluates GEOS-Chem-TOMAS particle number concentrations against
10 measurements and shows that including the extra SOA yields improved number predictions for
11 a wide range of particle sizes. The sensitivity of this additional source of SOA is also
12 investigated in this study.

13 We test the sensitivity of predicted size distributions to anthropogenically driven changes
14 in BVOC emissions in GEOS-Chem-TOMAS using twelve simulations. Table 1 shows the
15 assumptions in these twelve simulations. All simulations were run using 2005 meteorology with
16 three months of spin-up from a pre-spun-up restart file.

17 AE2 (Anthropogenic Emissions 2000) simulations use anthropogenic emissions for the
18 year 2005 and AEO (Anthropogenic Emissions Off) simulations (used to simulate an
19 atmosphere more similar to pre-industrial) have anthropogenic emissions off. BE1 (Biogenic
20 Emissions 1000) simulations use year 1000 biogenic emissions and BE2 (Biogenic Emissions
21 2000) simulations use year 2000 biogenic emissions for SOA production only. Changing the
22 biogenic emissions allows us to investigate the influence of changes to fixed-yield SOA
23 formation only and not to the changes in atmospheric oxidants (and the subsequent changes to
24 aerosols) associated with these changes in BVOC emissions. For gas-phase chemistry,
25 emissions of BVOCs are from online MEGAN for 2005 (Wainwright et al., 2012). Using the AE2
26 and AEO simulations, we can see if the sensitivity of aerosols and radiative forcing to changes
27 in BVOC emissions is strongly sensitive to the presence of anthropogenic aerosols. First, we
28 assume present-day anthropogenic emissions and have simultaneous monthly mean BVOC
29 emissions from MEGAN for the year 1000 (BE1.AE2.meg) and another simulation for the year
30 2000 also using MEGAN (BE2.AE2.meg) (the justification of these time periods is explained in
31 section 2.3). This method isolates the change in BVOCs and the effect on aerosol size
32 distributions under fixed anthropogenic emissions. We also test the sensitivity to changes in
33 BVOC emissions over the same periods with no anthropogenic emissions to simulate a pre-
34 industrial anthropogenic environment using MEGAN (BE1.AEO.meg and BE2.AEO.meg) and

1 LPJ-GUESS (BE1.AEO.LPJ and BE2.AEO.LPJ). Using these simulations, we also test the
2 sensitivity of predicted size distributions to changes in anthropogenic emissions under present-
3 day BVOC emissions from MEGAN by comparing simulations (BE2.AEO.meg and
4 BE2.AE2.meg). Thus, we estimate the effects of changing biogenic emissions in sets of
5 simulations where the anthropogenic emissions are either on or off. While neither of these
6 comparisons is realistic (anthropogenic emissions changed as the biogenic emissions were
7 changing), it allows us to bound the impact of anthropogenic emissions on the partial derivative
8 with respect to changing biogenic emissions.

9 We also test the model sensitivity to changes in SOA yields (as described previously)
10 over the same periods by repeating the four simulations using MEGAN (BE1.AE2.meg,
11 BE1.AEO.meg, BE2.AE2.meg and BE2.AEO.meg) with upper bounds on the SOA yields (10%,
12 20% and 40% of isoprene, monoterpenes and sesquiterpenes respectively) (BE1.AE2.up,
13 BE1.AEO.up, BE2.AE2.up, BE2.AEO.up). Finally, we investigate the sensitivity to the inclusion
14 of an additional 100 Tg yr^{-1} of anthropogenically enhanced SOA (as described previously) to the
15 simulations with present-day anthropogenic emissions using MEGAN biogenic emissions for
16 year-1000 and year-2000 conditions (BE1.XSOA, BE2.XSOA). We note that the predicted size
17 distributions and uncertainty ranges in this paper are sensitive to the nucleation scheme,
18 anthropogenic emissions fluxes and emissions size (e.g. Pierce et al. 2009c), but here we
19 explore the modeled partial derivatives to changes in BVOC emissions only.

20

21 **3.2 Aerosol direct effect and the cloud-albedo aerosol indirect effect**

22 The aerosol direct radiative effect (DRE) and the cloud-albedo (first) aerosol indirect effect (AIE)
23 in this study are calculated using an offline version of the Edwards and Slingo (ES) radiative
24 transfer model (Edwards and Slingo, 1996) which has been used previously in other aerosol
25 microphysics studies (Spracklen et al. 2011a; Rap et al. 2013; Pierce et al. 2013; Scott et al.
26 2014). The ES radiative transfer model uses monthly mean cloud climatology and surface
27 albedo, from the International Satellite Cloud Climatology Project (ISCCP) (Rossow and
28 Schiffer, 1999), for the year 2000. Note that the land-use changes that lead to the changes in
29 BVOC emissions explored in this paper may also lead to surface albedo and/or cloud changes;
30 however, we do not explore these changes in this paper.

31 To investigate the changes in DRE, an offline version of the RADAER module from the
32 Hadley Centre Global Environment Model (Bellouin et al., 2013) was adapted to calculate
33 aerosol optical parameters from GEOS-Chem-TOMAS output. The refractive index for each
34 size section is calculated as the volume-weighted mean refractive index of the components

1 (given at 500 nm in Table A1 of Bellouin et al., 2011), including water. Water uptake is tracked
2 explicitly in GEOS-Chem-TOMAS by using ISSOROPIA (Nenes et al., 1998). For
3 computational efficiency, the optical properties (dimensionless asymmetry parameter, and
4 scattering and absorption coefficients, in $\text{m}^2 \text{kg}^{-1}$) are then obtained from look-up tables of all
5 realistic combinations of refractive index and Mie parameter (particle radius normalized to
6 wavelength), as described by Bellouin et al. (2013). These aerosol optical properties were then
7 included in monthly climatologies when running the offline ES radiative transfer model.

8 The cloud-albedo AIE is calculated by perturbing the effective radii of cloud droplets in
9 the ES radiative transfer model. A control cloud droplet effective radius (r_{e1}) of $10 \mu\text{m}$ is
10 assumed uniformly, to maintain consistency with the ISCCP derivation of liquid water path, and
11 for each experiment a perturbed field of effective radii (r_{e2}) for low- and mid-level (below 600
12 hPa) water clouds are calculated as in Eq. (1) using the control ($CDNC_1$) and perturbed
13 ($CDNC_2$) fields of cloud droplet number concentration for each month.

$$r_{e2} = r_{e1} \times \left[\frac{CDNC_1}{CDNC_2} \right]^{1/3} \quad (1)$$

16
17 We calculate monthly mean CDNC using the aerosol size distributions predicted by
18 GEOS-Chem-TOMAS and a mechanistic parameterization of cloud drop formation from Nenes
19 and Seinfeld (2003), for a globally uniform updraft velocity of 0.2 m s^{-1} . The assumption of a
20 globally uniform updraft velocity is in itself a simplification and the AIE we calculate will be
21 sensitive to the value used. Spracklen et al. (2011) and Pierce et al. (2013) found that
22 assuming a base value of 0.2 m s^{-1} gave an AIE close to the mean AIE obtained when the
23 globally uniform updraft velocity was varied between 0.1 and 0.5 m s^{-1} . The cloud-albedo AIE is
24 then calculated by comparing the perturbed (using r_{e2}) net radiative fluxes at the top of the
25 atmosphere, to a control simulation (using r_{e1}).

26 The DRE and cloud-albedo AIE are approximately additive, but to give a combined
27 aerosol radiative effect, one must account for spatial overlap; therefore, a combined aerosol
28 radiative effect is calculated by perturbing the cloud droplet effective radii and aerosol
29 climatologies at the same time in the ES radiative transfer model, and comparing the net
30 radiative fluxes to a control simulation in which neither is perturbed.

31 32 **4 Results**

1 4.1 Changes to SOA formation rates

2 Figure 2a and b show the mean millennial fixed-yield SOA formation from MEGAN BVOC
3 emissions (monoterpenes, isoprene, and sesquiterpenes) and LPJ-GUESS BVOC emissions
4 (monoterpenes and isoprene) respectively in $\text{mg m}^{-2} \text{day}^{-1}$ over the years 1000-2000 and the
5 base SOA yield assumptions. Figures 2c and 2e show the absolute and relative change in
6 fixed-yield SOA formation from the same MEGAN BVOC emissions between 1000 and 2000
7 (year 2000 – year 1000), respectively. Figures 2d and 2f show the absolute and relative change
8 in fixed-yield SOA formation from the same LPJ-GUESS BVOC emissions between 1000 and
9 2000 (year 2000 – year 1000), respectively. An increase in SOA formation with time is
10 represented by red colors, and a decrease in SOA formation by blue. Globally, the mean SOA
11 formation from the MEGAN BVOC emissions decreases by 13.2% and decreases by 18.9%
12 from the LPJ-GUESS BVOC emissions. Regions such as central North America, eastern
13 Australia, and southern South America show significant decreases, exceeding 75% in SOA
14 formation from the MEGAN BVOC emissions. There are also regions such as India, and
15 southeast Asia with increases of greater than 50% in SOA formation from the MEGAN BVOC
16 emissions. These changes in emissions are largely due to millennial anthropogenic influences
17 on BVOC emissions through land-use changes. In Figure 2e, there are regions with large
18 percent increases or decreases in SOA formation, such as western North America and northern
19 Asia; however, the absolute change is negligible in these regions due to very low emissions.
20 SOA formation from LPJ-GUESS BVOC emissions generally exhibits the same spatial pattern
21 as MEGAN emissions. Where there are significant decreases/increases in BVOC emissions
22 from 1000 to 2000, there are corresponding decreases/increases in SOA formation.
23 Decreases/increases in SOA formation exceeding 50% would significantly decrease/increase
24 the amount of low-volatility condensable organic material available to grow nanoparticles in the
25 atmosphere. Therefore, changes in SOA formation of this magnitude could have an important
26 anthropogenic aerosol effect on regional climates.

27 Changes over the past millennium in all three classes of terpenoid BVOCs (Figure 1)
28 combine to impact SOA formation in the atmosphere. Figure 3 shows the percent contribution
29 to SOA formation by (a) isoprene, (b) monoterpene, and (c) sesquiterpene emissions using
30 MEGAN BVOC emissions, averaged over the years 1000-2000. The area enclosed by the red
31 contour represents regions with SOA formation rates greater than 5% of the maximum mean
32 millennial SOA formation from emissions of all BVOCs (isoprene + monoterpenes +
33 sesquiterpenes). Isoprene (Figure 3a) has the largest contribution to SOA formation with a
34 global millennial mean contribution of 64%. Regions where isoprene emissions have significant

1 contributions to SOA formation (greater than 70%) are collocated with regions of highest total
2 SOA formation (red contour). This shows that isoprene emissions are the predominant
3 simulated source of global biogenic SOA formation, despite having the lowest SOA production
4 yield of the three BVOCs. Some global models (e.g. D'Andrea et al. 2013; Lee et al. 2013) use
5 monoterpene emissions as a representative BVOC for SOA formation rather than isoprene
6 which may introduce errors in the spatial distribution and amount of biogenic SOA.
7 Monoterpene emissions (Figure 3b) contribute to 20% of global mean millennial SOA formation.
8 Figure 3b indicates that monoterpene emissions are the most important source of SOA in the
9 northern hemisphere boreal-forested regions, with contributions exceeding 80%. However,
10 monoterpenes contribute less than 20% in regions with the highest total SOA formation.
11 Sesquiterpene emissions represent the smallest global mean contribution to SOA formation at
12 16% over the past millennium. Unlike isoprene and monoterpene emissions that have clear
13 regional importance, Figure 3c indicates that sesquiterpene emissions tend to have a more
14 uniform contribution to SOA formation across all vegetated regions, but rarely exceeding 20%.

15

16 **4.2 Impact on aerosol number: changing BVOC emissions**

17 Table 2 summarizes the predicted global changes in particle number concentrations for all
18 comparisons to follow. Figure 4 shows the change in (a) N3, (b) N10, (c) N40, and (d) N80
19 (number of particles with diameter greater than 3 nm, 10 nm, 40 nm, and 80 nm respectively)
20 when changing MEGAN BVOC emissions from year 1000 to year 2000 with constant present
21 day anthropogenic emissions (2005) (BE2.AE2.meg – BE1.AE2.meg). (We use N40 and N80
22 as proxies for the number of CCN-sized particles. However, the actual CCN and cloud droplet
23 number concentrations depend on the maximum supersaturation reached in the cloud, which in
24 turn depends on updraft velocities and particle concentrations.) Comparing these two
25 simulations isolates the effect of millennial changes in BVOC emissions on particle size
26 distributions. Globally averaged, N3 and N10 increased by 2.3% and 1.5% respectively,
27 whereas N40 and N80 decreased by 0.6% and 1.3% respectively (see Table 2).

28 There are decreases in N80 exceeding 25% in regions such as southern South America,
29 southern Africa, southeastern North America and Australia. These regions coincide with
30 regions of significant decrease in isoprene emissions (Figure 1) and SOA formation (Figure 2).
31 The relationship between the decrease in isoprene emissions and SOA formation with the
32 decrease in N80 and increase in N3 and N10 can be explained through microphysical feedback
33 mechanisms. Firstly, the decrease in total isoprene emissions in these regions causes a
34 decrease in SOA formation as explained in section 4.1. With decreases in SOA formation,

1 ultrafine particle growth decreases due to the reduction in available condensable material. This
2 can be seen in Figure 4a and 4b where increases in N3 and N10 are collocated. This
3 suppression of ultrafine particle growth limits the number of particles that can grow to CCN
4 sizes, hence decreasing N80 in these regions. A reduction in the number of N80 reduces the
5 coagulation sink of smaller particles, and N3 and N10 increase. This can be seen in Figure 4,
6 where regions of increasing N3 and N10 coincide with regions of decreasing N40 and N80.
7 Throughout these regions, N3 and N10 increases exceed 25%, and decreases in N40 and N80
8 exceed 25%. These are significant changes in CCN concentrations (N40 and N80) in these
9 regions due largely to changes in BVOCs due to anthropogenic land-use changes. With
10 significant decreases in N40 and N80, the condensation sink for sulfuric acid (H_2SO_4) and
11 coagulation sink for ultrafine particles also decreases. This increases the survival probability of
12 ultrafine particles and hence increases N3 and N10. Secondly, with a decrease in SOA
13 formation and a decrease in ultrafine particle growth, the concentration of sulfuric acid (H_2SO_4)
14 vapor increases in these regions due to a decrease in the condensation sink. This increases
15 nucleation due to the strong dependence on H_2SO_4 vapor concentrations. Therefore, increased
16 nucleation increases the number of freshly nucleated particles and N3.

17 There are also increases in N80 over oceanic regions downwind of regions with
18 significant decreases in N80. This is caused by the increases in N3 and N10 over land. When
19 the air mass is advected over the ocean, the surplus of small particles are able to grow via
20 condensation to CCN sizes. Figure 5 shows the zonal-mean percentage change in (a) N3, (b)
21 N10, (c) N40, and (d) N80 when changing MEGAN BVOC emissions from year 1000 to year
22 2000 with constant present day anthropogenic emissions (2005) (BE2.AE2.meg –
23 BE1.AE2.meg). Figure 5 indicates that the difference in number concentrations between the
24 two simulations varies with height. The difference in N3 and N10 between the simulations with
25 height generally remains positive above the BL, with increases exceeding 5% in the southern
26 mid-latitudes in oceanic and deforested regions particularly. However, the differences in N40
27 and N80 between the simulations reverse sign with height in the mid-latitudes, most
28 dramatically in the southern hemisphere such that there are more particles in the BE2.AE2.meg
29 simulation. When CCN-sized particles are removed through wet deposition during vertical
30 advection, there are more ultrafine particles in the BE2.AE2.meg than the BE1.AE2.meg
31 simulation to grow to CCN sizes and replace the lost CCN. This feedback leads to the change
32 in sign with height for N40 and N80. This reversal in the change in particle number
33 concentrations has implications on the radiative forcing and will be discussed in section 4.3.

1 Figure 6 shows the change in (a) N3, (b) N10, (c) N40, and (d) N80 when changing
2 MEGAN BVOC emissions from year 1000 to year 2000 with anthropogenic emissions turned off
3 (BE2.AEO.meg – BE1.AEO.meg). Globally averaged, N3, N10, and N40 increased by 3.2%,
4 1.9%, and 0.4% respectively, whereas N80 decreased by 0.6% (see Table 2). Similar to the
5 previous case, globally averaged N3 and N10 increased over the past millennium. However,
6 contrary to the previous case, with anthropogenic emissions turned off globally averaged N40
7 also increased. The spatial patterns in globally averaged number of CCN sized particles (N80)
8 in this simulation reflected the same decreasing trend as Figure 4. In Figure 6, the regions of
9 increasing N3 and N10 coincide with regions of decreasing N40 and N80, following the same
10 spatial pattern as Figure 4. Thus, the presence of anthropogenic aerosols does not qualitatively
11 change the fractional response of the aerosol size distribution to millennial changes in BVOCs.

12 The microphysical feedback mechanisms in this comparison (BE2.AEO.meg –
13 BE1.AEO.meg) are the same as the previous comparison (BE2.AE2.meg – BE1.AE2.meg);
14 however, the magnitude of the changes in particle number concentrations due to BVOCs differs.
15 With anthropogenic emissions turned off to simulate pre-industrial conditions, changes in
16 number concentrations of particles in all size ranges are shifted towards more positive changes
17 than the simulation with present day anthropogenic emissions. This is caused by the difference
18 in total particle number concentrations and the mean size of the particles. As seen in Figure 7,
19 present-day anthropogenic conditions have more than 4 times more particles by number than
20 the pre-industrial conditions and the mean diameter is at smaller sizes. The mean diameter in
21 the simulation with present-day anthropogenic conditions is 30.6 nm, whereas the simulation
22 with pre-industrial anthropogenic conditions had a mean diameter of 52.1 nm. Therefore, there
23 are an increased number of ultrafine particles competing for condensation of SOA and growth to
24 CCN sizes in the simulations with anthropogenic emissions on, and the particles in these
25 simulations are (on average) smaller and further from CCN sizes. Thus, ultrafine particles grow
26 to CCN sizes more efficiently in the simulations with anthropogenic emissions turned off and are
27 more susceptible to BVOC emission changes because there are fewer particles competing for
28 condensable material and the mean size is larger. The fractional changes in N3 are larger in
29 the cases with anthropogenic emissions off because there are fewer particles overall. Thus,
30 there is a smaller increase in N3 and larger decrease in N80 than with anthropogenic emissions
31 turned off.

32 The effect on particle numbers by changing anthropogenic emissions under fixed BVOC
33 emissions was also investigated (not shown). The globally averaged change in N3, N10, N40,
34 and N80 when changing anthropogenic emissions from pre-industrial (off) to present-day (2005)

1 with constant present-day BVOC emissions (average biogenic emissions from 1980-1990)
2 (BE2.AE2.meg – BE2.AEO.meg) increased by 382%, 339%, 212%, and 162% respectively.
3 These global sensitivities to anthropogenic emissions changed only modestly when biogenic
4 emissions from 1000 were used (BE1.AE2.meg – BE1.AEO.meg): globally averaged N3, N10,
5 N40 and N80 all increased by 386%, 341%, 215%, and 164% respectively. The global millennial
6 change in particles due to BVOC changes is small compared to the change in anthropogenic
7 emissions; however, the change in particles due to changes in BVOC is still non-trivial, and we
8 will discuss this further when discussing radiative forcing. This emphasizes the importance of
9 accurately quantifying the aerosols in the pre-industrial reference state used for radiative forcing
10 calculations (Carslaw et al., 2013)

11 The sensitivity of particle numbers to upper bounds on SOA yields was also
12 investigated. The fixed SOA yields used in the standard simulations (3%, 10%, and 20% for
13 isoprene, monoterpenes, and sesquiterpenes respectively) were increased to 10%, 20%, and
14 40% for isoprene, monoterpenes, and sesquiterpenes respectively in the upper bound
15 simulations (BE2.AEO.up, BE1.AEO.up, BE2.AE2.up, and BE1.AE2.up). When using the upper
16 bound SOA yields and changing MEGAN BVOC emissions from year 1000 to year 2000 with
17 anthropogenic emissions turned off (BE2.AEO.up – BE1.AEO.up), globally averaged N3, N10,
18 N40, and N80 increased by 4.6%, 2.6%, 1.1%, and 0.0% respectively (see Table 2). The spatial
19 distribution of the global changes in particle number concentrations are similar to those of
20 Figure 4, with modest increases in magnitude. Even with more than a doubling of the SOA
21 yields from all three terpenoid species, the change in particle number responded with less than
22 a doubling due to microphysical dampening. This has also been observed in other global
23 aerosol microphysics models (e.g. Scott et al., 2014). With an increase in SOA yields, there is a
24 corresponding increase in the amount of condensable material available for particle growth.
25 However, due to the nonlinear balance between condensational growth and coagulation
26 scavenging, increases in particle number concentrations do not scale linearly with increases in
27 SOA formation.

28 This microphysical feedback was also seen when using upper bound SOA yields while
29 changing MEGAN BVOC emissions from year 1000 to year 2000 with present-day
30 anthropogenic emissions (2005) (BE2.AE2.up – BE1.AE2.up). Globally averaged, N3 and N10
31 increased by 3.6% and 2.6% respectively, whereas N40 and N80 decreased by 0.0% and 1.2%
32 respectively (see Table 2). This comparison showed the same spatial patterns as the standard
33 yield comparison of Figure 6 with modest increases in magnitude similar to the simulations with
34 anthropogenic emissions off. The nonlinear impact on global particle number concentrations

1 due to microphysical dampening was also observed in this comparison. Therefore, due to the
2 similarity of the upper bound SOA yield simulations to the standard SOA yield simulations, we
3 have not included the figures. However, the SOA yields will also likely not remain constant
4 since they will change with varying conditions such as aerosol loading or NO_x concentrations.

5 The sensitivity of particle numbers to historical changes in BVOC emissions with the
6 inclusion of an additional 100 Tg yr^{-1} of anthropogenically enhanced SOA as per D'Andrea et al.
7 (2013) was also investigated. The additional SOA used here may be SOA from BVOCs
8 enhanced by anthropogenic pollution; however we are leaving this additional SOA source
9 constant for both year 1000 and year 2000 biogenic emission simulations as an additional
10 sensitivity study. Figure 8 shows the change in (a) N3, (b) N10, (c) N40, and (d) N80 when
11 changing MEGAN BVOC emissions from year 1000 to year 2000 with constant present day
12 anthropogenic emissions including the additional $100 \text{ Tg (SOA) yr}^{-1}$ (BE2.XSOA – BE1.XSOA).
13 Globally averaged, N3, N10, and N40 increased by 1.9%, 1.2%, and 0.3% respectively,
14 whereas N80 decreased by 0.3% (see Table 2). The changes in particle number concentrations
15 with the additional $100 \text{ Tg (SOA) yr}^{-1}$ are lower in magnitude than the standard case
16 (BE2.AE2.meg – BE1.AE2.meg). With the inclusion of the additional SOA, there is a large
17 increase in the amount of condensable material available for particle growth. Therefore, the
18 smallest particles are able to grow more efficiently via condensation to larger sizes. This can be
19 seen in Figure 7 where the mean diameter for the simulation BE2.XSOA is 85.9 nm as opposed
20 to 30.6 nm for BE2.AE2.meg. However, the change in SOA from changes in BVOC emissions
21 is an order of magnitude lower than the additional anthropogenically enhanced SOA, therefore
22 the global changes in particle number concentrations when comparing the additional SOA cases
23 (BE2.XSOA – BE1.XSOA) to the standard cases (BE2.AE2.meg – BE1.AE2.meg) are lower in
24 magnitude (see Table 2).

25 Figure 9 shows the change in (a) N3, (b) N10, (c) N40, and (d) N80 when changing LPJ-
26 GUESS BVOC emissions from year 1000 to year 2000 with anthropogenic emissions off
27 (BE2.AEO.LPJ – BE1.AEO.LPJ) providing an estimate for the aerosol changes when using an
28 independent estimate of BVOC changes. Globally averaged, N3 and N10 increased by 5.9%
29 and 3.5% respectively, whereas N40 and N80 decreased by 0.1% and 1.8% respectively (see
30 Table 2). The magnitude of the changes in N3 and N80 with the LPJ-GUESS simulations are
31 highest of all the simulations. This is due in part to the spatial variability in the LPJ-GUESS
32 emission inventory when compared to the MEGAN emission inventory, as well as lower total
33 emissions. Similar to the comparable simulations using the MEGAN emissions (BE2.AEO.meg
34 – BE1.AEO.meg; Figure 6), there are increases in N3 over central North America, southern

1 South America, eastern Australia, and central Eurasia exceeding 25%. These regions
2 correspond to regions of decreased BVOC emissions over the past millennium, which leads to
3 decreases in SOA formation and increases in N3 (due to the deficit of condensable material
4 available to grow the smallest particles to CCN sizes). The same regions with significant
5 increases in N3 also correspond to regions of significant decreases in CCN sized particles.
6 However, there are regions where the MEGAN simulations and the LPJ-GUESS simulations
7 differ. Even though LPJ-GUESS emits less BVOC emissions globally than MEGAN, the LPJ-
8 GUESS simulations indicate higher magnitude increases in N3 in the Northern Hemisphere than
9 MEGAN. This is due to LPJ-GUESS emitting relatively more BVOCs in the northern boreal-
10 forested regions than MEGAN (largely due to the different emission factors assumed for
11 vegetation types and the treatment of the CO₂-response of the two emission models), and
12 therefore increased SOA formation. This is reflected in the global mean size distribution (Figure
13 7) where it can be seen that BE2.AEO.LPJ has fewer small particles than BE2.AEO.meg,
14 confirmed by a larger mean diameter at 63.6 nm as opposed to 52.1 nm for BE2.AEO.meg.
15 Overall, the percent change in N80 between the LPJ-GUESS and MEGAN simulations have a
16 correlation coefficient of 0.49. The previously mentioned regional differences between the two
17 BVOC reconstructions are a source of uncertainty, but the global percent change in N80 both
18 follow the same trend (Table 2). This indicates that anthropogenic land-use changes over the
19 past millennium have decreased the number of CCN sized particles globally through changes in
20 BVOC emissions, with regional changes in CCN sized particles ranging from -25% to 25%.

21 The distribution of changes across all grid boxes in N3, N10, N40, and N80 for all
22 simulations are summarized in Figure 10 (see Table 2 for specific values). Plotted are the
23 global percent changes in N3, N10, N40, and N80 for biogenic emissions from 1000 to 2000 on
24 a logarithmic scale. For all of the simulation comparisons, there is an increase in mean N3 and
25 a decrease in mean N80. This is due mainly to the decrease in isoprene emissions over the
26 past millennium, predominantly influenced by land-use changes. However, the majority of the
27 changes globally are very close to zero (as can be seen by the size of the interquartile range on
28 all plots). This is caused by minute changes in number concentrations over open ocean
29 regions. Also, there is significant variability in the magnitude of the changes in all simulations as
30 can be seen by the extent of the maximum and minimum changes in particle number
31 concentrations. This indicates that caution must be taken when interpreting global mean
32 values, as regional changes are of importance.

33

34 **4.3 Aerosol direct and indirect radiative effects**

1 Figure 11 shows the annual mean radiative effect due to changes in BVOC emissions between
2 year 1000 and year 2000 (see Table 3 for summarization). Figure 11a shows the DRE due to
3 changing BVOC emissions between year 1000 and year 2000 with MEGAN BVOC emissions
4 and anthropogenic emissions off (BE2.AEO.meg – BE1.AEO.meg); giving a global annual mean
5 DRE of $+0.065 \text{ W m}^{-2}$. While this global-mean DRE from biogenic emissions changes is smaller
6 in magnitude than estimated anthropogenic direct radiative forcings (e.g. estimates of -0.85 to
7 $+0.15 \text{ W m}^{-2}$ in the most recent IPCC report (Boucher et al., 2013)), the DRE from biogenic
8 emissions changes may be much larger, regionally. Throughout most oceanic regions, the DRE
9 is small ($<0.05 \text{ W m}^{-2}$); however, over land there are large regions experiencing a DRE greater
10 than $+0.5 \text{ W m}^{-2}$ (eg. southeastern South America, southern Africa, Australia, and southeastern
11 North America). This is caused by significant decreases in N80 (as seen in Figure 6) and the
12 total mass of particles (not shown), which decreases the scattering of incoming solar radiation.
13 There are regions of negative radiative forcing (eg. India), which are associated with increases
14 in N80 and total aerosol mass due to increased BVOC emissions from the anthropogenic
15 introduction of high BVOC emitting plants and cropland. There is a band of positive radiative
16 forcing in the southern hemisphere, which is associated with mid-latitude westerlies transporting
17 accumulation-mode particles over oceanic regions.

18 Figure 11b shows the DRE due to changing BVOC emissions between year 1000 and
19 year 2000 with LPJ-GUESS BVOC emissions and anthropogenic emissions off (BE2.AEO.LPJ
20 – BE1.AEO.LPJ), giving a global annual mean DRE of $+0.022 \text{ W m}^{-2}$. Similar to Figure 11a, the
21 DRE is very small ($<0.05 \text{ W m}^{-2}$) over most of the globe, in particular oceanic regions. However,
22 over BVOC source regions, the DRE exceeds $+0.3 \text{ W m}^{-2}$ due to decrease in isoprene
23 emissions and N80 in those regions. The DRE obtained using emissions from LPJ-GUESS is
24 spatially similar to that obtained with the MEGAN emissions, albeit lower in magnitude (due to
25 smaller emissions changes). However, there is a large difference in DRE between MEGAN and
26 LPJ-GUESS over Australia. This is due to a decrease in emissions from MEGAN between year
27 1000 and year 2000, resulting in a decrease in SOA formation and leading to a strong positive
28 DRE. However, there are smaller magnitude changes in emissions from LPJ-GUESS, which
29 are due to a combination of inland increases and coastal decreases (mainly caused by changes
30 in isoprene emissions), leading to a combination of increases and decreases in N80 over
31 Australia.

32 Figure 11c shows the cloud-albedo AIE due to changing BVOC emissions between year
33 1000 and year 2000 with MEGAN BVOC emissions and anthropogenic emissions off
34 (BE2.AEO.meg – BE1.AEO.meg), giving a global annual mean cloud-albedo AIE of -0.020 W m^{-2}

1 ². Similar to DRE above, the global-mean AIE from biogenic emissions changes is smaller than
2 estimated aerosol indirect forcings from anthropogenic aerosols (e.g. -0.3 to -1.8 W m⁻² in IPCC
3 AR4 (Forster et al., 2007)), but again the regional AIE from biogenic emissions changes can be
4 significantly larger than the mean. There is a band of negative radiative forcing associated with
5 increases in N80 in both the southern hemisphere and northern hemisphere mid-latitude
6 westerlies with regional cloud-albedo AIEs in excess of -0.10 W m⁻². The subtropical marine
7 clouds in these regions are sensitive to changes in CCN number concentration, giving a strong
8 cooling effect. This band of negative radiative forcing is caused by increased number
9 concentrations of CCN-sized particles (N40 and N80) above the BL (Figure 5). The increases in
10 CCN-sized particles aloft causes increases in CDNC in the vertical layers with the highest cloud
11 fractions (~700 hPa) and thus a net cooling effect. There are also regions that experience a
12 small positive cloud-albedo AIE due to changing BVOC emissions (e.g. southeastern North
13 America, western Europe, and southeastern Australia) associated with regions of decreased
14 N80.

15 Figure 11d shows the cloud-albedo AIE due to changing BVOC emissions between year
16 1000 and year 2000 with LPJ-GUESS BVOC emissions and anthropogenic emissions off
17 (BE2.AEO.LPJ – BE1.AEO.LPJ), giving a global annual mean cloud-albedo AIE of -0.008 W m⁻².
18 ². The global annual mean cloud-albedo AIE calculated using the LPJ-GUESS emissions is
19 lower in magnitude than that calculated using the MEGAN emissions. This occurs because the
20 LPJ-GUESS simulations exhibit smaller decreases in N80 over the oceanic regions when
21 compared to the MEGAN simulations. There is also a stronger warming effect over regions
22 such as central North America, southeastern South America, central Africa, and central Eurasia
23 due to the decrease in N80. Figure 11e shows the combined aerosol radiative effect due to
24 changing BVOC emissions between year 1000 and year 2000 with MEGAN BVOC emissions
25 and anthropogenic emissions off (BE2.AEO.meg – BE1.AEO.meg) with a global mean warming
26 of +0.049 W m⁻². The cooling effect from the cloud-albedo AIE (Figure 11c) over oceanic
27 regions tends to be approximately canceled out due to the warming effect from the DRE (Figure
28 11a), and the regional warming effect from the DRE dominates the total radiative effect. Figure
29 11f shows the combined aerosol radiative effect due to changing BVOC emissions between
30 year 1000 and year 2000 with LPJ-GUESS BVOC emissions and anthropogenic emissions off
31 (BE2.AEO.LPJ – BE1.AEO.LPJ) with a global mean warming of +0.015 W m⁻². Similar to Figure
32 11e, the AIE cooling effect over oceanic regions is balanced by the warming effect in the same
33 regions due to the increases in DRE. Therefore, the warming effect from the DRE dominates
34 the total radiative effect. The additional significance of Figure 11 is that it shows the forcing

1 error resulting from holding biological emissions fixed when calculating anthropogenic radiative
2 forcings from pre-industrial to present day. Thus, the error in the anthropogenic forcing maybe
3 on the order of 0.5 W m^{-2} over various regions if these changes in biogenic emissions are not
4 included.

5 We also explored the aerosol radiative effect under the assumption of upper bound SOA
6 yields. With this upper bound yield changing MEGAN BVOC emissions from year 1000 to year
7 2000 with present-day anthropogenic emissions (2005) (BE2.AE2.up – BE1.AE2.up) resulted in
8 a global mean DRE of $+0.163 \text{ W m}^{-2}$ (a factor 3.2 greater than under standard SOA yields) and
9 the global mean cloud-albedo AIE to -0.056 W m^{-2} (factor 1.6 greater than standard SOA yield).
10 The radiative effect due to changing BVOC emissions is therefore sensitive to assumptions
11 about SOA yield.

12

13 **4.4 Discussion of model limitations**

14 There are certain limitations associated with our assumptions and model setup used in this
15 study. Organic emissions do not participate in the nucleation process within GEOS-Chem-
16 TOMAS, however the inclusion of oxidized organic vapors may increase the sensitivity of
17 particle number concentrations to changes in BVOC emissions, particularly in monoterpene-
18 emitting regions known to produce extremely low volatile organic compounds (Riccobono et al.,
19 2014, Scott et al., 2014). This inclusion of organic vapors in the nucleation process would also
20 increase the pre-industrial (year 1000) baseline number concentrations (Scott et al., 2014). The
21 SOA yields in GEOS-Chem-TOMAS are fixed; however, these yields may change with total
22 organic mass, NO_x concentrations, and changes in atmospheric oxidants. The change in SOA
23 formation has no influence on the oxidation fields in GEOS-Chem-TOMAS and therefore there
24 may be missing feedback mechanisms on key atmospheric oxidants as BVOCs are removed
25 from the model system without changing model OH concentrations. This model also ignores
26 OH recycling mechanisms that may accompany changes in isoprene oxidation, which may
27 impact oxidation rates and SOA yields. SOA formation by NO_3 is not included in this model -
28 while this is likely minor for much of the globe, we may be underestimating SOA formed in areas
29 influenced by monoterpenes and NO_x . Also, the inclusion of an additional 100 Tg yr^{-1} of
30 anthropogenically enhanced SOA is relevant for present day conditions; however, it's likely not
31 representative of the pre-industrial atmosphere. This change in anthropogenically enhanced
32 SOA will cause additional uncertainties in our predictions, by changing the organic aerosol
33 mass, which affect SOA growth rates and yields. The BVOC reconstructions also inherently
34 have uncertainties associated with them. The response of plant emissions to environmental

1 changes including CO₂ and temperature is contentious, particularly with respect to monoterpene
2 and sesquiterpene emission. Plant BVOC emissions respond differently to CO₂ exposure in the
3 short-term versus CO₂ exposure in the long-term. (i.e. BVOC emissions of plants exposed to
4 elevated CO₂ for minutes or hours are different from BVOC emissions plants exposed to
5 elevated CO₂ from seed germination) (Heald et al., 2009). Perhaps more important for this
6 study, the temperature dependence of BVOC emissions included in the emission models are
7 typically based on short-term leaf-level exposure, and ignore the potential for plants to adapt to
8 increasing temperature. Both MEGAN and LPJ-GUESS have been separately evaluated
9 against observations (Arneth et al., 2007; Schurgers et al., 2009; Guenther et al., 2006) and
10 compared to each other (Arneth et al., 2011; Guenther et al., 2012), however without long-term
11 measurements of BVOC fluxes there may be bias in the reconstructions towards the available
12 short-term measurements used to develop the reconstructions. Experimental limitations in
13 emission factors for the various plant functional types used to create the reconstruction also
14 lead to uncertainties in the BVOC reconstructions. Finally, there is no way to directly test the
15 emissions for the historic simulations. We expect the general spatial patterns to be robust, not
16 necessarily the magnitudes.

17

18 **5 Conclusions**

19 In this study, we investigated the impact of millennial changes in biogenic volatile organic
20 compound (BVOC) emissions on secondary organic aerosol (SOA) formation, global aerosol
21 size distributions and calculated the associated aerosol radiative forcing. We used the global
22 aerosol microphysics model GEOS-Chem-TOMAS to connect the historical changes in BVOC
23 emissions to particle size distributions and the number concentration of cloud condensation
24 nuclei (CCN).

25 This study built off recent work by Acosta Navarro et al. (2014) who determined how
26 BVOC emissions have changed in the past millennium due to changes in land use, temperature,
27 and carbon dioxide (CO₂) concentrations. They used two model reconstructions including three
28 dominant classes of BVOC emissions (isoprene, monoterpenes, and sesquiterpenes) to
29 simulate decadal-averaged monthly mean emissions over the time period 1000-2000. Their
30 emissions reconstructions predicted that isoprene emissions decreased over the past
31 millennium (due mainly to anthropogenic land-use changes), whereas monoterpene and
32 sesquiterpene emissions increased (due predominantly to temperature increases). In our work,
33 we included these millennial emissions into the GEOS-Chem-TOMAS chemical-transport model
34 with online aerosol microphysics for SOA production only (no influence on the oxidant fields).

1 We assumed that isoprene, monoterpenes, and sesquiterpenes form SOA in GEOS-Chem-
2 TOMAS via fixed yields of 3%, 10%, and 20% respectively.

3 When anthropogenic emissions (eg. SO_2 , NO_x , primary aerosols) were turned off to
4 represent pre-industrial conditions and emissions of isoprene, monoterpenes, and
5 sesquiterpenes changed from year 1000 values (“pre-industrial”) to year 2000 values (“present
6 day”) using both BVOC reconstructions, N80 (the number of particles with diameter greater than
7 80 nm, our proxy for CCN in this study) had decreases of greater than 25% in year 2000 relative
8 to year 1000 that were predicted in regions with extensive land-use changes such as southern
9 South America, southern Africa, southeastern North America and southeastern Australia since
10 year 1000. This significant change in N80 was predominantly driven by anthropogenic changes
11 in high BVOC-emitting vegetation to lower emitting crops/grazing land. Similar sensitivities in
12 N80 exist when BVOC emissions were changed over the same time period but with
13 anthropogenic emissions set to present day values. Including recent work by Spracklen et al.
14 (2011a) and D’Andrea et al. (2013), the sensitivity to an additional 100 Tg yr^{-1} of
15 anthropogenically enhanced SOA was tested, with BVOC emissions changed from year 1000 to
16 year 2000 values, resulting in globally averaged decreases in N80 of 0.3%. However, similar to
17 the previous simulations, there are regional decreases exceeding 25%. The sensitivity to SOA
18 yields was also investigated by comparing simulations for year 1000 and 2000 BVOC emissions
19 (with anthropogenic emissions both on and off) by increasing the yields from the base case 3%,
20 10%, and 20% for isoprene, monoterpenes, and sesquiterpenes respectively, to 10%, 20%, and
21 40% respectively. This significant increase (at least a doubling) in SOA formation resulted in a
22 nonlinear increase in the magnitude of the changes in particle number concentrations of all
23 sizes (doubling yields did not double changes in particle number concentrations); however,
24 confirmed the same trend by globally decreasing N80. There are uncertainties in assuming
25 fixed SOA yields however, as SOA yields are dependent on conditions such as aerosol loading
26 and NO_x concentrations, and therefore might not be fixed with time.

27 The aerosol radiative effects associated with this millennial change in BVOC emissions
28 were also investigated. Globally, with anthropogenic emissions off and changing BVOC
29 emissions from year 1000 to 2000, there is an annual mean $+0.065 \text{ W m}^{-2}$ warming due to the
30 aerosol direct effect (decrease in scattering of incoming solar radiation from decreased number
31 concentrations of N80). However, there are regions such as southeastern South America,
32 southern Africa, and Australia where the warming effect due to the DRE exceeds $+0.50 \text{ W m}^{-2}$.
33 The cloud albedo (first) aerosol indirect effect was also calculated for the same simulations
34 indicating a global annual mean cloud-albedo AIE of -0.020 W m^{-2} , with most cooling effect

1 occurring over oceanic regions (with high sensitivities and susceptibilities to changes in cloud
2 properties) due to a small increase in N80 downwind of regions decreased BVOC emissions.

3 There are substantial uncertainties in emissions of BVOC and SOA yield. Additionally,
4 the magnitude of the forcing of the biogenic changes differs whether anthropogenic emissions
5 are on or off. When we account for these uncertainties the net global mean DRE due to
6 millennial change in BVOC emissions is estimated to be between +0.022 and +0.163 $W m^{-2}$ and
7 the net global mean cloud-albedo AIE is estimated to be between -0.008 and -0.056 $W m^{-2}$. Our
8 calculated range in direct effect brackets the +0.09 $W m^{-2}$ global mean DRE recently estimated
9 by Unger (2014), where biogenic emissions changed only due to year 1850 to 2000
10 anthropogenic land-use change. Overall, we find that millennial changes in BVOC emissions
11 warm the climate, with the combined radiative effect (DRE plus cloud-albedo AIE) estimated to
12 be between +0.015 and +0.118 $W m^{-2}$. We therefore find that anthropogenic land-use change,
13 which dominates our calculated changes to BVOC emissions, warms climate through reducing
14 the SOA burden. Reductions in BVOC emissions also impact other short-lived climate forcers
15 (SLCF) including O_3 , OH, and CH_4 (Unger, 2014). However, the large uncertainty in the aerosol
16 radiative effect precludes an accurate assessment of the net impact of land-use change on
17 climate through SLCFs. Improved understanding of the atmospheric impacts of BVOCs is
18 required before the net impact of land-use change on climate through SLCFs can be accurately
19 determined. Research priorities include improved understanding of BVOC oxidation
20 mechanisms, SOA yields including interactions with anthropogenic emissions and the role of
21 BVOC oxidation products in particle formation.

22 The changes in CCN due to millennial changes in BVOC emissions are predicted to be
23 non-trivial in many regions, however other uncertainties influencing CCN number concentrations
24 must also be considered (Lee et al., 2013), such as nucleation mechanisms (Pierce and Adams,
25 2009c; Reddington et al., 2011; Spracklen et al., 2008; Wang and Penner, 2009), amount and
26 volatility of SOA (Spracklen et al., 2011a; Riipinen et al., 2011; D'Andrea et al., 2013), amount
27 and size of primary emissions (Adams and Seinfeld, 2003; Pierce and Adams, 2006, 2007,
28 2009c; Reddington et al., 2011; Spracklen et al., 2011a), and wet deposition (Croft et al., 2012).

29 While present-day emissions of anthropogenic aerosols are a significant contributor to
30 climate change, this study has shown the importance of anthropogenically driven changes in
31 BVOC emissions over the past millennium on SOA formation, CCN number concentrations, and
32 radiative forcing. The large decrease in CCN due to land-use changes over the past millennium
33 appears to be a largely overlooked and important anthropogenic aerosol effect on regional
34 climates. Finally, these results show that present-day BVOC emissions should not be used in

1 pre-industrial aerosol simulations as they may cause errors in the reference state of the
2 atmosphere when calculating the radiative forcing due to anthropogenic activities.

3
4
5
6

7 **Acknowledgements**

8 We thank the Atlantic Computational Excellence Network (ACENet) for the computational
9 resources used in this study. The authors acknowledge Natural Sciences and Engineering
10 Research Council (NSERC) of Canada for funding through the Network on Climate and
11 Aerosols (NETCARE) network. Financial support from the European Research Council (ERC-
12 StG-ATMOGAIN grant no: 278277) and Vetenskapsrådet (grant no: 2011-5120) and Natural
13 Environment Research Council (grant number NE/K015966/1) is gratefully acknowledged.

14

15 **References**

16 Acosta Navarro, J. C., Smolander, S., Struthers, H., Zorita, E., Ekman, A. M. L., Kaplan, J. O.,
17 Guenther, A., Arneth, A. and Riipinen, I.: Global emissions of terpenoid VOCs from terrestrial,
18 *Journal of Geophysical Research-Atmospheres*, 6867–6885, doi:10.1002/2013JD021238, 2014.

19

20 Adams, P. J. and Seinfeld, J. H.: Disproportionate impact of particulate emissions on global
21 cloud condensation nuclei concentrations, *Geophys. Res. Lett.*, 30, 1210–1239,
22 doi:10.1029/2002GL016303, 2003.

23

24 Arneth, A., Niinemets, Ü., Pressley, S., Bäck, J., Hari, P., Karl, T., Noe, S., Prentice, I. C.,
25 Serça, D., Hickler, T., Wolf, A., and Smith, B.: Process-based estimates of terrestrial ecosystem
26 isoprene emissions: incorporating the effects of a direct CO₂-isoprene interaction, *Atmos. Chem.*
27 *Phys.*, 7, 31-53, doi:10.5194/acp-7-31-2007, 2007.

28

29 Arneth, A., Schurgers, G., Lathiere, J., Duhl, T., Beerling, D. J., Hewitt, C. N., Martin, M., and
30 Guenther, A.: Global terrestrial isoprene emission models: sensitivity to variability in climate and
31 vegetation, *Atmos. Chem. Phys.*, 11, 8037-8052, doi:10.5194/acp-11-8037-2011, 2011.

32

33 Bellouin, N., Rae, J., Jones, A., Johnson, C., Haywood, J. and Boucher, O.: Aerosol forcing in
34 the Climate Model Intercomparison Project (CMIP5) simulations by HadGEM2-ES and the role
35 of ammonium nitrate, *J. Geophys. Res. Atmospheres*, 116(D20), D20206,
36 doi:10.1029/2011JD016074, 2011.

37 Bellouin, N., Mann, G. W., Woodhouse, M. T., Johnson, C., Carslaw, K. S., and Dalvi, M.:
38 Impact of the modal aerosol scheme GLOMAP-mode on aerosol forcing in the Hadley
39 Centre Global Environmental Model, *Atmos. Chem. Phys.*, 13, 3027–3044,
40 doi:10.5194/acp-13-3027-2013, 2013.

1 Benkovitz, C. M., Scholtz, M. T., Pacyna, J., Tarrason, L., Dignon, J., Voldner, E. C., Spiro, P.
2 A., Logan, J. A., and Graedel, T. E.: Global gridded inventories of anthropogenic emissions of
3 sulfur and nitrogen, *J. Geophys. Res.*, 101, 29 239–29 254, 1996.
4
5 Boucher, O., D. Randall, P. Artaxo, C. Bretherton, G. Feingold, P. Forster, V.-M. Kerminen, Y.
6 Kondo, H. Liao, U. Lohmann, P. Rasch, S.K. Satheesh, S. Sherwood, B. Stevens, X. Y. Z.:
7 Clouds and Aerosols, in *Climate Change 2013: The Physical Science Basis. Contribution of*
8 *Working Group I to the Fifth Assessment Report of the Intergovernmental Panel on Climate*
9 *Change*, edited by J. B. Stocker, T.F., D. Qin, G.-K. Plattner, M. Tignor, S.K. Allen and P. M. M.
10 A. Nauels, Y. Xia, V. Bex, Cambridge University Press, Cambridge, United Kingdom and New
11 York, NY, USA., 2013.
12
13 Carlton, A. G., Wiedinmyer, C., and Kroll, J. H.: A review of Secondary Organic Aerosol (SOA)
14 formation from isoprene, *Atmos. Chem. Phys.*, 9, 4987-5005, doi:10.5194/acp-9-4987-2009,
15 2009.
16
17 Carslaw, K. S., Lee, L. a, Reddington, C. L., Pringle, K. J., Rap, a, Forster, P. M., Mann, G. W.,
18 Spracklen, D. V, Woodhouse, M. T., Regayre, L. a and Pierce, J. R.: Large contribution of
19 natural aerosols to uncertainty in indirect forcing., *Nature*, 503(7474), 67–71,
20 doi:10.1038/nature12674, 2013.
21
22 Chameides, W. L., Lindsay, R. W., Richardson, J., and Kiang, C. S: The Role of Biogenic
23 Hydrocarbons in Urban Photochemical Smog: Atlanta as a Case Study, *Science*, 241, 1473–
24 1475, 1998.
25
26 Charlson, R. J., Schwartz, S. E., Hales, J. M., Cess, R. D., Coakley Jr., J. A., Hansen, J. E. and
27 Hofmann, D. J.: Climate forcing by anthropogenic aerosols, *Science*, 255(5043), 423-430, 1992.
28 Clement, A. C., Burgman, R., and Norris, J. R.: Observational and Model Evidence for Positive
29 Low-Level Cloud Feedback, *Science*, 325, 460–464, 2009.
30
31 Croft, B., Pierce, J. R., Martin, R. V., Hoose, C., and Lohmann, U.: Uncertainty associated with
32 convective wet removal of entrained aerosols in a global climate model, *Atmos. Chem. Phys.*,
33 12, 10725-10748, doi:10.5194/acp-12-10725-2012, 2012.
34
35 Donahue, N. M., Trump, E. R., Pierce, J. R. and Riipinen, I.: Theoretical constraints on pure
36 vapor-pressure driven condensation of organics to ultrafine particles, *Geophysical Research*
37 *Letters*, 38(16), L16801, doi:10.1029/2011GL048115, 2011.
38
39 Dusek, U., Frank, G.P., Hildebrandt, L., Curtius, J., Schneider, J., Walter, S., Chand, D.,
40 Drewnick, F., Hings, S., Jung, D., Borrmann, S., Andreae, M.O.: Size Matters More Than
41 Chemistry for Cloud-Nucleating Ability of Aerosol Particles, *Science* 312, 1375-1378, 2006.
42
43 Edwards, J. M. & Slingo, A.: Studies with a flexible new radiation code. I: Choosing a
44 configuration for a large-scale model, *Quarterly Journal of the Royal Meteorological Society*,
45 122, 689-719, 1996.

1
2 Ehn, M., Thornton, J. a, Kleist, E., Sipilä, M., Junninen, H., Pullinen, I., Springer, M., Rubach, F.,
3 Tillmann, R., Lee, B., Lopez-Hilfiker, F., Andres, S., Acir, I.-H., Rissanen, M., Jokinen, T.,
4 Schobesberger, S., Kangasluoma, J., Kontkanen, J., Nieminen, T., Kurtén, T., Nielsen, L. B.,
5 Jørgensen, S., Kjaergaard, H. G., Canagaratna, M., Maso, M. D., Berndt, T., Petäjä, T.,
6 Wahner, A., Kerminen, V.-M., Kulmala, M., Worsnop, D. R., Wildt, J. and Mentel, T. F.: A large
7 source of low-volatility secondary organic aerosol., *Nature*, 506(7489), 476–9,
8 doi:10.1038/nature13032, 2014.
9
10 Forster, P., Ramaswamy, V., Artaxo, P., Berntsen, T., Betts, R., Fahey, D. W., Haywood, J.,
11 Lean, J., Lowe, D. C., Myhre, G., Nganga, J., Prinn, R., Raga, G., Schulz, M. and Dorland, R. V:
12 Changes in atmospheric constituents and in radiative forcing, in *Climate change 2007: the*
13 *physical science basis. contribution of working group I to the fourth assessment report of the*
14 *intergovernmental panel on climate change*, edited by S. Solomon, D. Qin, M. Manning, Z.
15 Chen, M. Marquis, K. B. Averyt, M. Tignor, and H. L. Miller, pp. 129–234, Cambridge University
16 Press, Cambridge, United Kingdom and New York, NY, USA., 2007.
17
18 Guenther, A., Karl, T., Harley, P., Wiedinmyer, C., Palmer, P. I., and Geron, C.: Estimates of
19 global terrestrial isoprene emissions using MEGAN (Model of Emissions of Gases and Aerosols
20 from Nature), *Atmos. Chem. Phys.*, 6, 3181-3210, doi:10.5194/acp-6-3181-2006, 2006.
21
22 Guenther, A. B., X. Jiang, C. L. Heald, T. Sakulyanontvittaya, T. Duhl, L. K. Emmons, and X.
23 Wang: The model of emissions of gases and aerosols from nature version 2.1 (megan2.1): an
24 extended and updated framework for modeling biogenic emissions, *Geoscientific Model*
25 *Development Discussions*, 5(2), 1503–1560, doi:10.5194/gmdd-5- 1503-2012, 2012.
26
27 Hallquist, M., Wenger, J. C., Baltensperger, U., Rudich, Y., Simpson, D., Claeys, M., Dommen,
28 J., Donahue, N. M., George, C., Goldstein, A. H., Hamilton, J. F., Herrmann, H., Hoffmann, T.,
29 Iinuma, Y., Jang, M., Jenkin, M. E., Jimenez, J. L., Kiendler-Scharr, A., Maenhaut, W.,
30 McFiggans, G., Mentel, Th. F., Monod, A., Prévôt, A. S. H., Seinfeld, J. H., Surratt, J. D.,
31 Szmigielski, R., and Wildt, J.: The formation, properties and impact of secondary organic
32 aerosol: current and emerging issues, *Atmos. Chem. Phys.*, 9, 5155–5236, doi:10.5194/acp-9-
33 5155-2009, 2009.
34
35 Heald, C. L., Henze, D. K., Horowitz, L. W., Feddema, J., Lamarque, J.-F., Guenther, a., Hess,
36 P. G., Vitt, F., Seinfeld, J. H., Goldstein, a. H. and Fung, I.: Predicted change in global
37 secondary organic aerosol concentrations in response to future climate, emissions, and land
38 use change, *J. Geophys. Res. Atmos.*, 113(D5), n/a–n/a, doi:10.1029/2007JD009092, 2008.
39
40 Bellouin, N., Rae, J., Jones, A., Johnson, C., Haywood, J. and Boucher, O.: Aerosol forcing in
41 the Climate Model Intercomparison Project (CMIP5) simulations by HadGEM2-ES and the role
42 of ammonium nitrate, *J. Geophys. Res. Atmospheres*, 116(D20), D20206,
43 doi:10.1029/2011JD016074, 2011.

1 Heald, C. L., Wilkinson, M. J., Monson, R. K., Alo, C. A., Wang, G. and Guenther, A.: Response
2 of isoprene emission to ambient CO₂ changes and implications for global budgets, *Glob.*
3 *Change Biol.*, 15(5), 1127–1140, doi:10.1111/j.1365-2486.2008.01802.x, 2009.

4

5 Jimenez, J. L., Canagaratna, M. R., Donahue, N. M., Prevot, A. S. H., Zhang, Q., Kroll, J. H.,
6 DeCarlo, P. F., Allan, J. D., Coe, H., Ng, N. L., Aiken, A. C., Docherty, K. S., Ulbrich, I. M.,
7 Grieshop, A. P., Robinson, A. L., Duplissy, J., Smith, J. D., Wilson, K. R., Lanz, V. A., Hueglin,
8 C., Sun, Y. L., Tian, J., Laaksonen, A., Raatikainen, T., Rautiainen, J., Vaattovaara, P., Ehn, M.,
9 Kulmala, M., Tomlinson, J. M., Collins, D. R., Cubison, M. J., Dunlea, E. J., Huffman, J. A.,
10 Onasch, T. B., Alfarra, M. R., Williams, P. I., Bower, K., Kondo, Y., Schneider, J., Drewnick, F.,
11 Borrmann, S., Weimer, S., Demerjian, K., Salcedo, D., Cottrell, L., Griffin, R., Takami, A.,
12 Miyoshi, T., Hatakeyama, S., Shimono, A., Sun, J. Y., Zhang, Y. M., Dzepina, K., Kimmel, J. R.,
13 Sueper, D., Jayne, J. T., Herndon, S. C., Trimborn, A. M., Williams, L. R., Wood, E. C.,
14 Middlebrook, A. M., Kolb, C. E., Baltensperger, U. and Worsnop, D. R.: Evolution of organic
15 aerosols in the atmosphere., *Science*, 326(5959), 1525–9, doi:10.1126/science.1180353, 2009.
16

17 Jung, J., Fountoukis, C., Adams, P. J. and Pandis, S. N.: Simulation of in situ ultrafine particle
18 formation in the eastern United States using PMCAMx-UF, *J. Geophys. Res.*, 115, D03203,
19 doi:10.1029/2009JD012313, 2010.

20

21 Kaplan, J. O., Krumhardt, K. M., Ellis, E. C., Ruddiman, W. F., Lemmen, C., and Goldewijk, K.
22 K.: Holocene carbon emissions as a result of anthropogenic land cover change, *The Holocene*,
23 21(5), 775-791, 2011.

24

25 Kanakidou, M., Seinfeld, J. H., Pandis, S. N., Barnes, I., Dentener, F. J., Facchini, M. C., Van
26 Dingenen, R., Ervens, B., Nenes, A., Nielsen, C. J., Swietlicki, E., Putaud, J. P., Balkanski, Y.,
27 Fuzzi, S., Horth, J., Moortgat, G. K., Winterhalter, R., Myhre, C. E. L., Tsigaridis, K., Vignati, E.,
28 Stephanou, E. G., and Wilson, J.: Organic aerosol and global climate modelling: a review,
29 *Atmos. Chem. Phys.*, 5, 1053-1123, doi:10.5194/acp-5-1053-2005, 2005.

30

31 Kerminen, V.-M. and Kulmala, M.: Analytical formulae connecting the “real” and the “apparent”
32 nucleation rate and the nuclei number concentration for atmospheric nucleation events, *J.*
33 *Aerosol Sci.*, 33, 609–622, 2002.

34

35 Kerminen, V.-M., Paramonov, M., Anttila, T., Riipinen, I., Fountoukis, C., Korhonen, H., Asmi,
36 E., Laakso, L., Lihavainen, H., Swietlicki, E., Svenningsson, B., Asmi, A., Pandis, S. N.,
37 Kulmala, M., and Petäjä, T.: Cloud condensation nuclei production associated with atmospheric
38 nucleation: a synthesis based on existing literature and new results, *Atmos. Chem. Phys.*, 12,
39 12037-12059, doi:10.5194/acp-12-12037-2012, 2012.

40

41 Kroll, J. H., and Seinfeld, J. H.: Chemistry of secondary organic aerosol: Formation and
42 evolution of low-volatility organics in the atmosphere, *Atmospheric Environment*, 42(16), 3593-
43 3624, 2008.

1 Kroll, J. H., Ng, N. L., Murphy, S. M., Flagan, R. C., and Seinfeld, J. H.: Secondary organic
2 aerosol formation from isoprene photooxidation under high-NO_x conditions, *Geophys. Res.
3 Lett.*, 40(6), 1869-1877, 2006.
4
5 Kuang, C., McMurry, P. H. and McCormick, A. V: Determination of cloud condensation nuclei
6 production from measured new particle formation events, *Geophysical Research Letters*, 36(9),
7 n/a–n/a, doi:10.1029/2009GL037584, 2009.
8
9 Kulmala, M., Vehkamäki, H., Petäjä, T., Dal Maso, M., Lauri, A., Kerminen, V.-M., Birmili, W.,
10 and McMurry, P. H.: Formation and growth of ultrafine atmospheric particles: A review of
11 observations, *J. Aerosol Sci.*, 35, 143–176, 2004.
12
13 Lamsal, L. N., Martin, R. V., Van Donkelaar, A., Steinbacher, M., Celarier, E. A., Bucsela, E.,
14 Dunlea, E. J., and Pinto, J. P.: Ground-level nitrogen dioxide concentrations inferred from the
15 satellite-borne Ozone Monitoring Instrument, *Journal of Geophysical Research: Atmospheres*
16 (1984–2012), 113(D16), 2008.
17
18 Lee, Y.H., and Adams, P. J.: A Fast and Efficient Version of the Two-Moment Aerosol
19 Sectional (TOMAS) Global Aerosol Microphysics Model, *Aerosol Science and Technology*, 46,
20 678-689, 10.1080/02786826.2011.643259, 2011.
21
22 Lee, L. A., Pringle, K. J., Reddington, C. L., Mann, G. W., Stier, P., Spracklen, D. V., Pierce, J.
23 R., and Carslaw, K. S.: The magnitude and causes of uncertainty in global model simulations of
24 cloud condensation nuclei, *Atmos. Chem. Phys.*, 13, 8879-8914, doi:10.5194/acp-13-8879-
25 2013, 2013.
26
27 Liao, L., Kerminen, V.-M., Boy, M., Kulmala, M., and Dal Maso, M.: Temperature influence on
28 the natural aerosol budget over boreal forests, *Atmos. Chem. Phys.*, 14, 8295-8308,
29 doi:10.5194/acp-14-8295-2014, 2014.
30
31 McFiggans, G., Artaxo, P., Baltensperger, U., Coe, H., Facchini, M. C., Feingold, G., Fuzzi, S.,
32 Gysel, M., Laaksonen, A., Lohmann, U., Mentel, T. F., Murphy, D. M., O'Dowd, C. D., Snider, J.
33 R., and Weingartner, E.: The effect of physical and chemical aerosol properties on warm cloud
34 droplet activation, *Atmos. Chem. Phys.*, 6, 2593-2649, doi:10.5194/acp-6-2593-2006, 2006.
35
36 Napari, I., Noppel, M., Vehkamäki, H. and Kulmala, M.: Parametrization of ternary nucleation
37 rates for H₂SO₄-NH₃-H₂O vapors, *Journal of Geophysical Research: Atmospheres*, 107(D19),
38 AAC 6–1–AAC 6–6, doi:10.1029/2002JD002132, 2002.
39
40 Nenes, A. and Seinfeld, J. H.: Parameterization of cloud droplet formation in global climate
41 models, *J. Geophys. Res.-Atmos.*, 108, 4415, doi:10.1029/2002JD002911, 2003.
42

1 Nenes, A., Pandis, S. N. and Pilinis, C.: ISORROPIA: A New Thermodynamic Equilibrium
2 Model for Multiphase Multicomponent Inorganic Aerosols, *Aquat. Geochem.*, 4(1), 123–152,
3 doi:10.1023/A:1009604003981, 1998.
4

5 Paasonen, P., Asmi, A., Petaja, T., Kajos, M. K., Aijala, M., Junninen, H., Holst, T., Abbatt, J. P.
6 D., Arneth, A., Birmili, W., van der Gon, H. D., Hamed, A., Hoffer, A., Laakso, L., Laaksonen, A.,
7 Leaitch, W. R., Plass-Dulmer, C., Pryor, S. C., Raisanen, P., Swietlicki, E., Wiedensohler, A.,
8 Worsnop, D. R., Kerminen, V.-M. and Kulmala, M.: Warming-induced increase in aerosol
9 number concentration likely to moderate climate change, *Nat. Geosci.*, 6(6), 438–442, 2013.
10

11 Pacifico, F., Folberth, G. A., Jones, C. D., Harrison, S. P., and Collins, W. J.: Sensitivity of
12 biogenic isoprene emissions to past, present, and future environmental conditions and implica-
13 tions for atmospheric chemistry, *J. Geophys. Res.*, 117, D22302, doi:10.1029/2012JD018276,
14 2012.
15

16 Peñuelas, J., and M. Staudt: BVOCs and global change, *Trends in Plant Science*, 15(3), 133 –
17 144, doi:http://dx.doi.org/10.1016/j.tplants.2009.12.005, Issue: Induced biogenic volatile organic
18 compounds from plants, 2010.
19

20 Petters, M. D. and Kreidenweis, S. M.: A single parameter representation of hygroscopic growth
21 and cloud condensation nucleus activity, *Atmos. Chem. Phys.*, 7, 1961-1971, doi:10.5194/acp-
22 7-1961-2007, 2007.
23

24 Pierce, J. R. and Adams, P. J.: Global evaluation of CCN formation by direct emission of sea
25 salt and growth of ultrafine sea salt, *Journal of Geophysical Research-Atmospheres*, 111(D6),
26 D06203, doi:10.1029/2005JD006186, 2006.
27

28 Pierce, J. R. and Adams, P. J.: Efficiency of cloud condensation nuclei formation from ultrafine
29 particles, *Atmospheric Chemistry and Physics*, 7, 1367–1379, 2007.
30

31 Pierce, J. R. and Adams, P. J.: Uncertainty in global CCN concentrations from uncertain aerosol
32 nucleation and primary emission rates, *Atmospheric Chemistry and Physics*, 9(4), 1339–1356,
33 doi:10.5194/acp-9-1339-2009, 2009c.
34

35 Pierce, J. R., Riipinen, I., Kulmala, M., Ehn, M., Petäjä, T., Junninen, H., Worsnop, D. R., and
36 Donahue, N. M.: Quantification of the volatility of secondary organic compounds in ultrafine
37 particles during nucleation events, *Atmos. Chem. Phys.*, 11, 9019-9036, doi:10.5194/acp-11-
38 9019-2011, 2011.
39

40 Pierce, J. R., Evans, M. J., Scott, C. E., D'Andrea, S. D., Farmer, D. K., Swietlicki, E., and
41 Spracklen, D. V.: Weak global sensitivity of cloud condensation nuclei and the aerosol indirect
42 effect to Criegee + SO₂ chemistry, *Atmos. Chem. Phys.*, 13, 3163-3176, doi:10.5194/acp-13-
43 3163-2013, 2013.
44

1 Pye, H. O. T., Chan, A. W. H., Barkley, M. P., and Seinfeld, J. H.: Global modeling of organic
2 aerosol: the importance of reactive nitrogen (NO_x and NO₃), *Atmos. Chem. Phys.*, 10, 11261-
3 11276, doi:10.5194/acp-10-11261-2010, 2010.

4 Rap, A., Scott, C. E., Spracklen, D. V., Bellouin, N., Forster, P. M., Carslaw, K. S., Schmidt, A.
5 and Mann, G.: Natural aerosol direct and indirect radiative effects. *Geophysical Research*
6 *Letters*, 40, 3297– 3301, 2013.

7

8 Reddington, C. L., Carslaw, K. S., Spracklen, D. V., Frontoso, M. G., Collins, L., Merikanto, J.,
9 Minikin, A., Hamburger, T., Coe, H., Kulmala, M., Aalto, P., Flentje, H., Plass-Dülmer, C., Birmili,
10 W., Wiedensohler, A., Wehner, B., Tuch, T., Sonntag, A., O'Dowd, C. D., Jennings, S. G.,
11 Dupuy, R., Baltensperger, U., Weingartner, E., Hansson, H.-C., Tunved, P., Laj, P., Sellegri, K.,
12 Boulon, J., Putaud, J.-P., Gruening, C., Swietlicki, E., Roldin, P., Henzing, J. S., Moerman, M.,
13 Mihalopoulos, N., Kouvarakis, G., Ždímal, V., Zíková, N., Marinoni, A., Bonasoni, P., and Duchi,
14 R.: Primary versus secondary contributions to particle number concentrations in the European
15 boundary layer, *Atmos. Chem. Phys.*, 11, 12007-12036, doi:10.5194/acp-11-12007-2011, 2011.

16

17 Riccobono, F., Schobesberger, S., Scott, C. E., Dommen, J., Ortega, I. K., Rondo, L., Almeida,
18 J., Amorim, A., Bianchi, F., Breitenlechner, M., David, A., Downard, A., Dunne, E. M., Duplissy,
19 J., Ehrhart, S., Flagan, R. C., Franchin, A., Hansel, A., Junninen, H., Kajos, M., Keskinen, H.,
20 Kupc, A., Kürten, A., Kvashin, A. N., Laaksonen, A., Lehtipalo, K., Makhmutov, V., Mathot, S.,
21 Nieminen, T., Onnela, A., Petäjä, T., Praplan, A. P., Santos, F. D., Schallhart, S., Seinfeld, J. H.,
22 Sipilä, M., Spracklen, D. V., Stozhkov, Y., Stratmann, F., Tomé, A., Tsagkogeorgas, G.,
23 Vaattovaara, P., Viisanen, Y., Vrtala, A., Wagner, P. E., Weingartner, E., Wex, H., Wimmer, D.,
24 Carslaw, K. S., Curtius, J., Donahue, N. M., Kirkby, J., Kulmala, M., Worsnop, D. R. and
25 Baltensperger, U.: Oxidation products of biogenic emissions contribute to nucleation of
26 atmospheric particles., *Science*, 344(6185), 717–21, doi:10.1126/science.1243527, 2014.

27

28 Riipinen, I., Pierce, J. R., Yli-Juuti, T., Nieminen, T., Häkkinen, S., Ehn, M., Junninen, H.,
29 Lehtipalo, K., Petäjä, T., Slowik, J., Chang, R., Shantz, N. C., Abbatt, J., Leitch, W. R.,
30 Kerminen, V.-M., Worsnop, D. R., Pandis, S. N., Donahue, N. M., and Kulmala, M.: Organic
31 condensation: a vital link connecting aerosol formation to cloud condensation nuclei (CCN)
32 concentrations, *Atmos. Chem. Phys.*, 11, 3865-3878, doi:10.5194/acp-11-3865-2011, 2011.

33

34 Riipinen, I., Yli-Juuti, T., Pierce, J. R., Petäjä, T., Worsnop, D. R., Kulmala, M., and Donahue,
35 N. M.: The contribution of organics to atmospheric nanoparticle growth, *Nature Geosci.*, 5, 453–
36 458, doi:10.1038/ngeo1499, 2012.

37

38 Rosenfeld, D., Lohmann, U., Raga, G. B., O'Dowd, C. D., Kulmala, M., Fuzzi, S., Reissell, A.,
39 and Andreae, M. O.: Flood or Drought: How Do Aerosols Affect Precipitation?, *Science*, 312,
40 1309–1313, 2008.

41

42 Rossow, W. B. and Schiffer, R. A.: Advances in understanding clouds from ISCCP, *B. Am.*
43 *Meteorol. Soc.*, 80, 2261–2288, 1999.

44

1 Schurgers, G., Hickler, T., Miller, P. A., & Arneth, A.: European emissions of isoprene and
2 monoterpenes from the Last Glacial Maximum to present, *Biogeosciences Discussions*, 6(5),
3 8805-8849, 2009.

4 Scott, C. E., Rap, A., Spracklen, D. V., Forster, P. M., Carslaw, K. S., Mann, G. W., Pringle, K.
5 J., Kivekäs, N., Kulmala, M., Lihavainen, H., and Tunved, P.: The direct and indirect radiative
6 effects of biogenic secondary organic aerosol, *Atmos. Chem. Phys.*, 14, 447-470,
7 doi:10.5194/acp-14-447-2014, 2014.

8

9 Sipilä, M., Berndt, T., Petäjä, T., Brus, D., Vanhanen, J., Stratmann, F., Patokoski, J., Mauldin
10 III, R. L., Hyvärinen, A.-P., Lihavainen, H., and Kulmala, M.: Role of Sulfuric Acid in Atmospheric
11 Nucleation, *Science*, 327, 1243–1246, 2010.

12

13 Sitch, S., Smith, B., Prentice, I. C., Arneth, A., Bondeau, A., Cramer, W., Kaplan, J. O., Levis,
14 S., Lucht, W., Sykes, M. T., Thonicke, K., and Venevsky, S.: Evaluation of ecosystem dynamics,
15 plant geography and terrestrial carbon cycling in the LPJ dynamic global vegetation model,
16 *Glob. Change Biol.*, 9(2), 161-185, 2003.

17

18 Smith, B., Prentice, I. C., and Sykes, M. T.: Representation of vegetation dynamics in the
19 modelling of terrestrial ecosystems: comparing two contrasting approaches within European
20 climate space, *Global Ecology & Biogeography*, 10, 621-637, 2001.

21

22 Spracklen, D. V., Carslaw, K. S., Kulmala, M., Kerminen, V. M., Sihto, S. L., Riipinen, I.,
23 Merikanto, J., Mann, G. W., Chipperfield, M. P., Wiedensohler, A., Birmili, W., and Lihavainen,
24 H.: Contribution of particle formation to global cloud condensation nuclei concentrations,
25 *Geophys. Res. Lett.*, 35, D06808, doi:10.1029/2007GL033038, 2008.

26

27 Spracklen, D. V., Carslaw, K. S., Poschl, U., Rap, A., and Forster, P. M.: Global cloud
28 condensation nuclei influenced by carbonaceous combustion aerosol, *Atmos. Chem. Phys.*, 11,
29 9067–9087, doi:10.5194/acp-11-9067-2011, 2011a.

30

31 Tanaka, K., Kim, H.-J., Saito, K., Takahashi, H. G., Watanabe, M., Yokohata, T., Kimoto, M.,
32 Takata, K., and Yasunari, T.: How have both cultivation and warming influenced annual global
33 isoprene and monoterpene emissions since the preindustrial era?, *Atmos. Chem. Phys.*, 12,
34 9703-9718, doi:10.5194/acp-12-9703-2012, 2012.

35

36 Unger, N.: Isoprene emission variability through the twentieth century, *J. Geophys. Res. Atmos.*,
37 118(24), 13,606–13,613, doi:10.1002/2013JD020978, 2013.

38

39 Unger, N.: Human land-use-driven reduction of forest volatiles cools global climate, ,
40 4(October), 907–910, doi:10.1038/NCLIMATE2347, 2014.

41

42 Van Donkelaar, A., Martin, R. V., Leaitch, W. R., Macdonald, A. M., Walker, T. W., Streets, D.
43 G., Zhang, Q., Dunlea, E. J., Jimenez, J. L., Dibb, J. E., Huey, L. G., Weber, R., and Andreae,
44 M. O.: Analysis of aircraft and satellite measurements from the Intercontinental Chemical

1 Transport Experiment (INTEX-B) to quantify long-range transport of East Asian sulfur to
2 Canada, *Atmos. Chem. Phys.*, 8, 2999–3014, doi:10.5194/acp-8-2999-2008, 2008.
3
4 Vehkamäki, H. and Riipinen, I.: Thermodynamics and kinetics of atmospheric aerosol particle
5 formation and growth, *Chemical Society Reviews*, 41(15), 5160-5173, doi:
6 10.1039/c2cs00002d, 2012.
7
8 Wainwright, C. D., Pierce, J. R., Liggio, J., Strawbridge, K. B., Macdonald, A. M., and Leitch,
9 R. W.: The effect of model spatial resolution on Secondary Organic Aerosol predictions: a case
10 study at Whistler, BC, Canada, *Atmos. Chem. Phys.*, 12, 10911-10923, doi:10.5194/acp-12-
11 10911-2012, 2012.
12
13 Wang, M. and Penner, J. E.: Aerosol indirect forcing in a global model with particle nucleation,
14 *Atmos. Chem. Phys.*, 9, 239-260, doi:10.5194/acp-9-239-2009, 2009.
15
16 Ward, D. S., Mahowald, N. M., and Kloster, S.: Potential climate forcing of land use and land
17 cover change, *Atmos. Chem. Phys. Discuss.*, 14, 12167-12234, doi:10.5194/acpd-14-12167-
18 2014, 2014.
19
20 Westervelt, D. M., Pierce, J. R., Riipinen, I., Trivitayanurak, W., Hamed, A., Kulmala, M.,
21 Laaksonen, A., Decesari, S., and Adams, P. J.: Formation and growth of nucleated particles into
22 cloud condensation nuclei: model-measurement comparison, *Atmos. Chem. Phys. Discuss.*, 13,
23 8333-8386, doi:10.5194/acpd-13-8333-2013, 2013.
24
25 Wu, S., Mickley, L. J., Kaplan, J. O., and Jacob, D. J.: Impacts of changes in land use and land
26 cover on atmospheric chemistry and air quality over the 21st century, *Atmos. Chem. Phys.*, 12,
27 1597-1609, doi:10.5194/acp-12-1597-2012, 2012.
28
29 Xu, L., Kollman, M. S., Song, C., Shilling, J. E., Ng, N. L.: "Effects of NO_x on the volatility of
30 secondary organic aerosol from isoprene photooxidation." *Environ. Sci. Technol.*, 48 (4), pp
31 2253–2262, DOI: 10.1021/es404842g, 2014.

1 Table 1. Summary of the GEOS-Chem-TOMAS simulations performed in this study. Biogenic
 2 emissions for year 1000 and 2000 using MEGAN are decadal-averaged emissions for 1000-
 3 1010 and 1980-1990 respectively, whereas LPJ-GUESS biogenic emissions are annual-
 4 averaged for the years 1000 and 2000. Standard SOA yields are 3%, 10% and 20% for
 5 isoprene, monoterpenes and sesquiterpenes respectively, and upper bound SOA yields are
 6 10%, 20% and 40% for isoprene, monoterpenes and sesquiterpenes respectively. In the
 7 simulation naming scheme, “BE” refers to biogenic emissions, “1” refers to year 1000, “2” refers
 8 to year 2000, “O” refers to off, “meg” refers to MEGAN BVOC emissions, “LPJ” refers to LPJ-
 9 GUESS BVOC emissions, “up” refers to upper bound SOA yields, and “XSOA” refers to the
 10 inclusion of the additional 100 Tg (SOA) yr⁻¹.

11

Simulation name	Biogenic emissions	Anthropogenic emissions	MEGAN (Acosta Navarro et al., 2014)	LPJ-GUESS (Acosta Navarro et al., 2014)	Standard SOA yield	Upper bound SOA yield	Additional 100 Tg (SOA) yr ⁻¹ (D’Andrea et al., 2013)	Total biogenic SOA formation rates (Tg yr ⁻¹)
BE1.AE2.meg	1000	YES	YES	NO	YES	NO	NO	35.96
BE1.AEO.meg	1000	NO	YES	NO	YES	NO	NO	35.96
BE2.AE2.meg	2000	YES	YES	NO	YES	NO	NO	41.44
BE2.AEO.meg	2000	NO	YES	NO	YES	NO	NO	41.44
BE1.AEO.LPJ	1000	NO	NO	YES	YES	NO	NO	13.63
BE2.AEO.LPJ	2000	NO	NO	YES	YES	NO	NO	16.81
BE1.AE2.up	1000	YES	YES	NO	NO	YES	NO	100.30
BE1.AEO.up	1000	NO	YES	NO	NO	YES	NO	100.30
BE2.AE2.up	2000	YES	YES	NO	NO	YES	NO	118.92
BE2.AEO.up	2000	NO	YES	NO	NO	YES	NO	118.92
BE1.XSOA	1000	YES	YES	NO	YES	NO	YES	135.96
BE2.XSOA	2000	YES	YES	NO	YES	NO	YES	141.44

12

1 Table 2. Summary of global, annual mean percent changes in N3, N10, N40 and N80 (number
 2 of particles with diameter greater than 3 nm, 10 nm, 40 nm and 80 nm respectively) when
 3 changing BVOC emissions from year 1000 to year 2000 using the MEGAN and LPJ-GUESS
 4 reconstructions. The values in brackets are the global maximum and minimum percent changes
 5 respectively.
 6

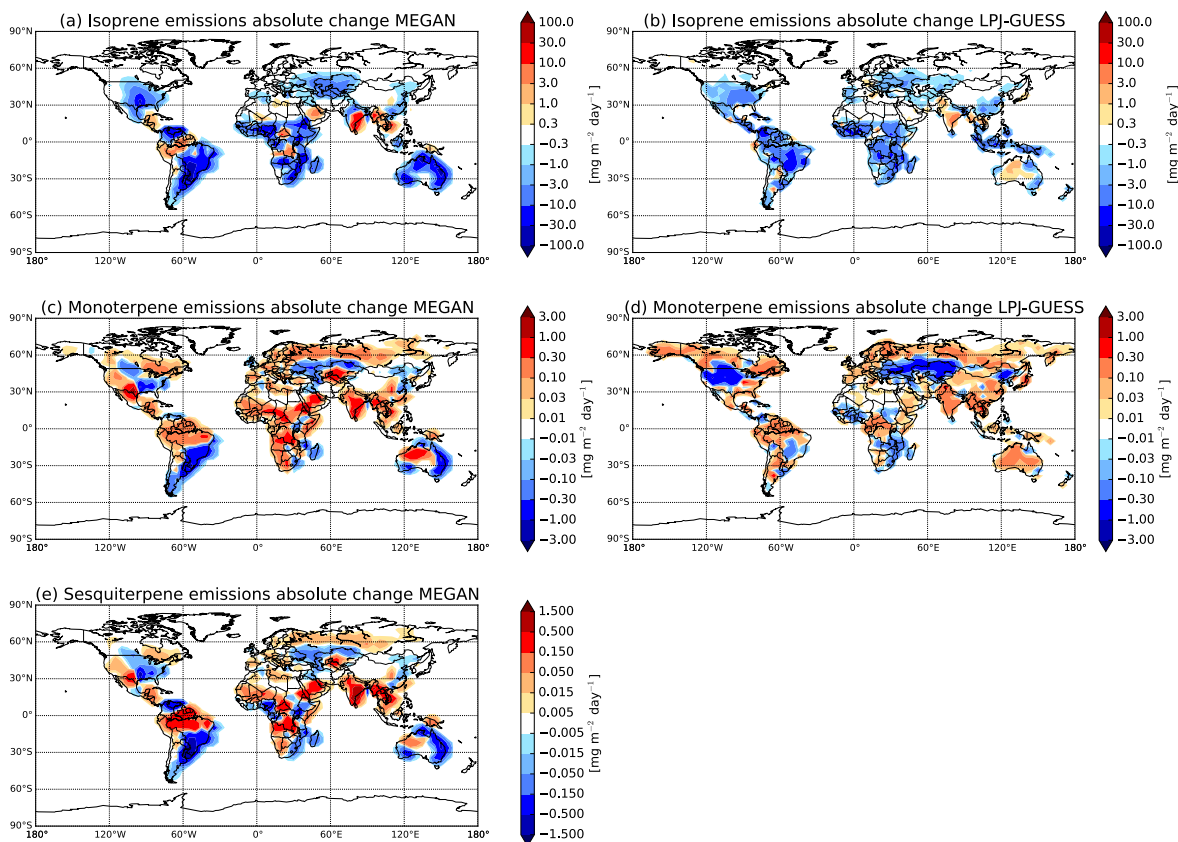
	MEGAN					LPJ-GUESS
	BE2.AEO – BE1.AEO	BE2.AE2 – BE1.AE2	BE2.AEO.up – BE1.AEO.up	BE2.AE2.up – BE1.AE2.up	BE2.XSOA – BE1.XSOA	BE2.AEO.LPJ – BE1.AEO.LPJ
N3	3.2% (40%, -10%)	2.3% (49%, -21%)	4.6% (53%, -10%)	3.6% (59%, -27%)	1.9% (26%, -3%)	5.9% (63%, -17%)
N10	1.9 % (38%, -25%)	1.5% (29%, -13%)	2.6% (40%, -29%)	2.6% (34%, -18%)	1.2% (17%, -2%)	3.5% (36%, -13%)
N40	0.4 % (28%, -23%)	-0.6% (18%, -42%)	1.1% (45%, -44%)	-0.0% (20%, -41%)	0.3% (8%, -14%)	-0.1% (24%, -28%)
N80	-0.6% (20%, -28%)	-1.3% (21%, -43%)	0.0% (33%, -24%)	-1.2% (25%, -40%)	-0.3% (5%, -21%)	-1.8% (34%, -36%)

7

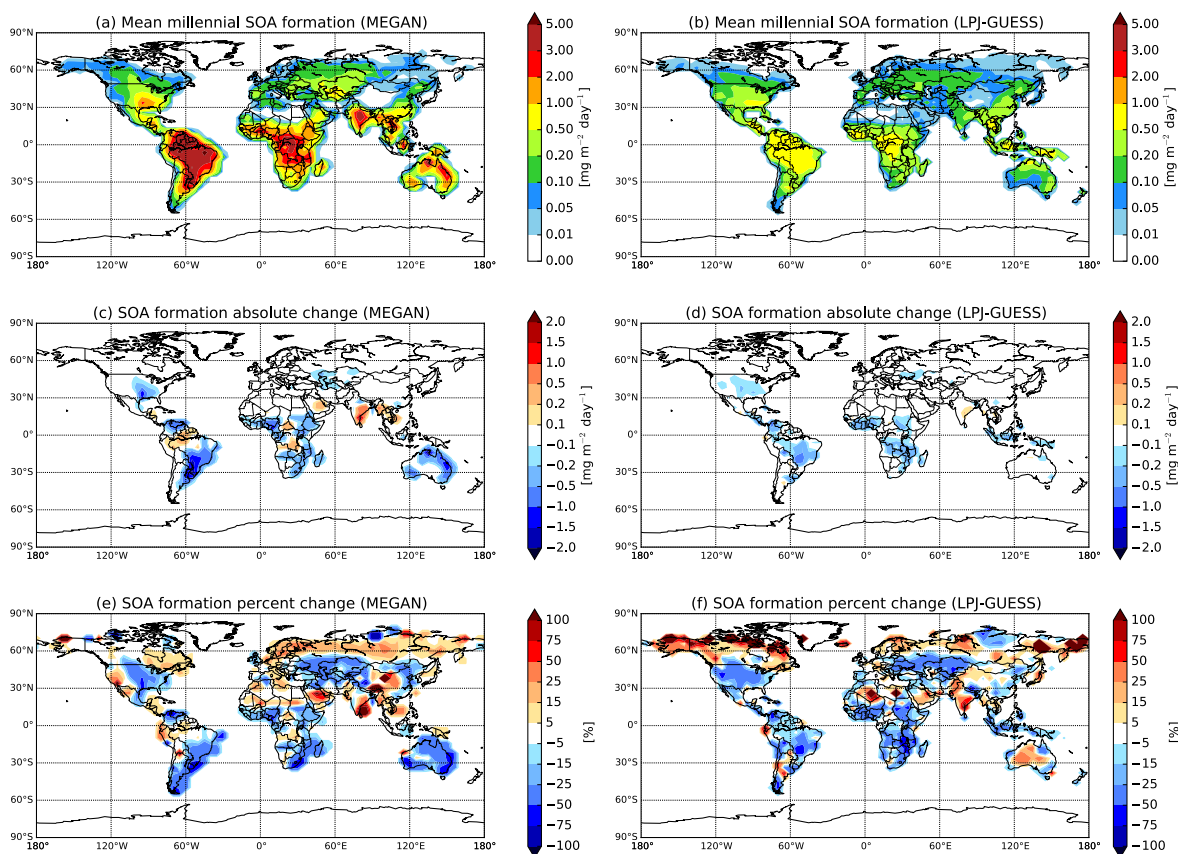
1 Table 3. Summary of global, annual mean changes in aerosol direct radiative effect (DRE), first
 2 aerosol indirect effect (AIE), and combined radiative effect in $W m^{-2}$ when changing BVOC
 3 emissions from year 1000 to year 2000 using the MEGAN and LPJ-GUESS reconstructions.
 4 The values in brackets are the global maximum and minimum changes respectively. *Cloud
 5 drop number concentrations were calculated using a globally uniform updraft velocity of $0.2 m s^{-1}$.
 6
 7

	MEGAN					LPJ-GUESS
	BE2.AEO – BE1.AEO	BE2.AE2 – BE1.AE2	BE2.AEO.up – BE1.AEO.up	BE2.AE2.up – BE1.AE2.up	BE2.XSOA – BE1.XSOA	BE2.AEO.LPJ – BE1.AEO.LPJ
DRE [$W m^{-2}$]	+0.065 (-0.305, +1.008)	+0.050 (-0.394, +1.005)	+0.129 (-0.521, +1.806)	+0.163 (-0.934, +2.020)	+0.052 (-0.377, +0.985)	+0.022 (-0.059, +0.381)
AIE* [$W m^{-2}$]	-0.020 (-0.175, +0.201)	-0.035 (-0.262, +0.406)	-0.035 (-0.291, +0.212)	-0.056 (-0.369, +0.154)	-0.025 (-0.288, +0.108)	-0.008 (-0.156, +0.285)
Combined Radiative Effect* [$W m^{-2}$]	+0.049 (-0.316, +1.019)	+0.022 (-0.394, +1.005)	+0.101 (-0.547, +1.808)	+0.118 (-0.930, +1.970)	+0.032 (-0.382, +0.973)	+0.015 (-0.122, +0.436)

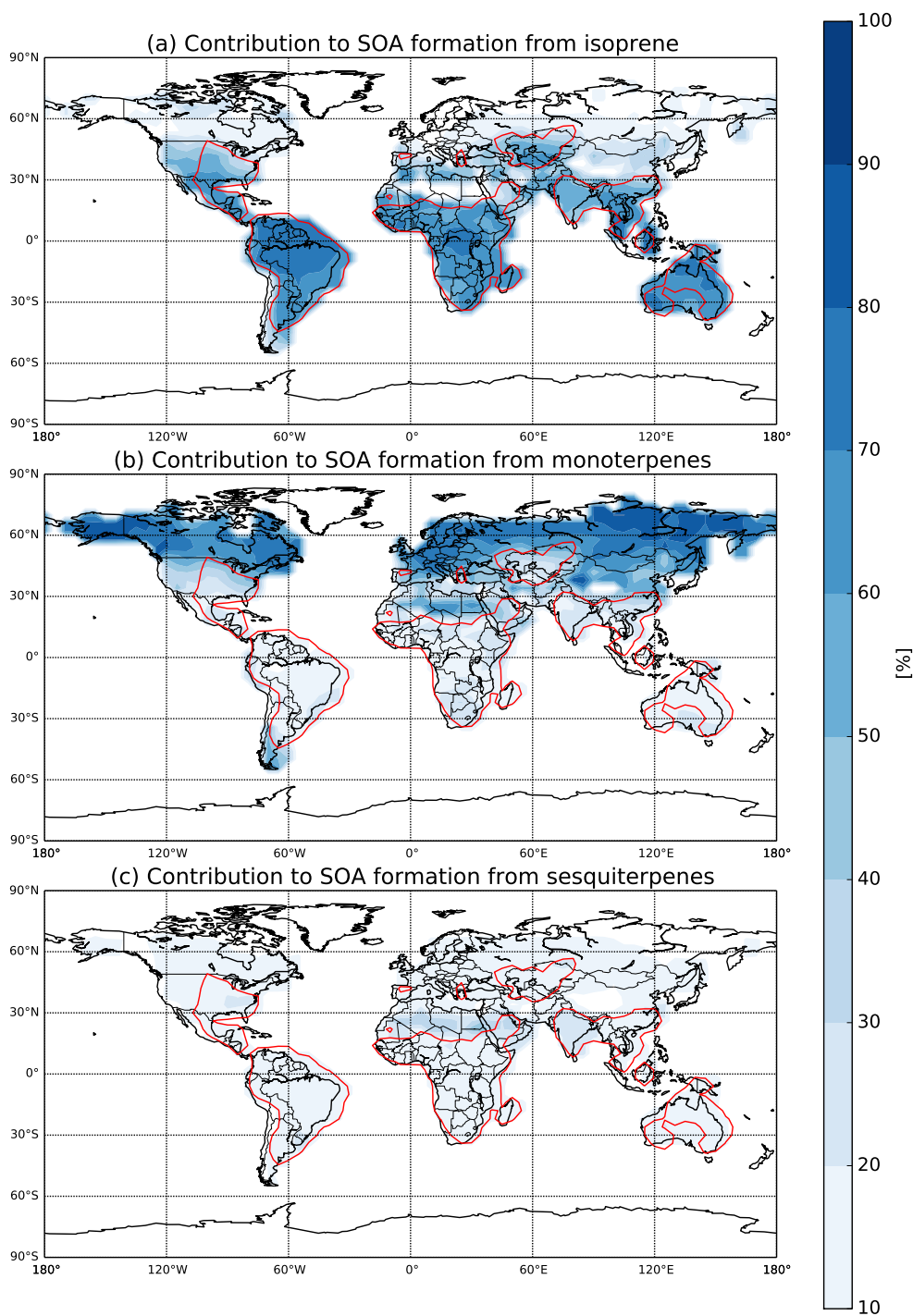
8



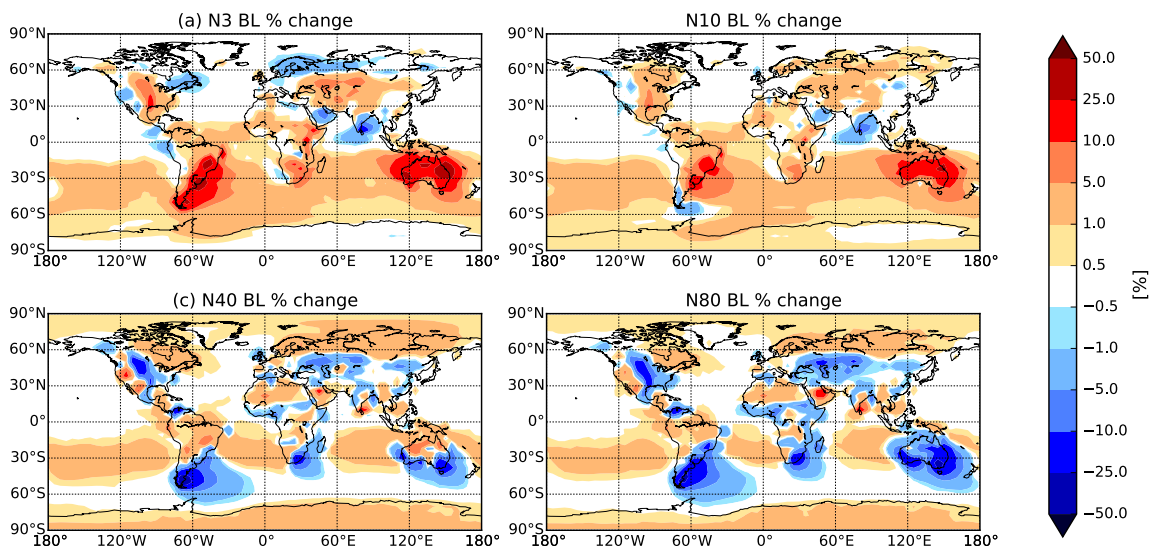
1
 2 Figure 1. Absolute change in (a) isoprene, (c) monoterpene, and (e) sesquiterpene emissions
 3 between the years 1000-1010 and 1980-1990 in $\text{mg m}^{-2} \text{ day}^{-1}$ from the MEGAN terpenoid
 4 reconstruction and absolute change in (b) isoprene, and (d) monoterpene emissions between
 5 the years 1000 and 2000 in $\text{mg m}^{-2} \text{ day}^{-1}$ from the LPJ-GUESS terpenoid reconstruction (Acosta
 6 Navarro et al., 2014). Note the change of scale between panels. An increase in emissions is
 7 represented by red colors, and a decrease in isoprene emissions by blue.



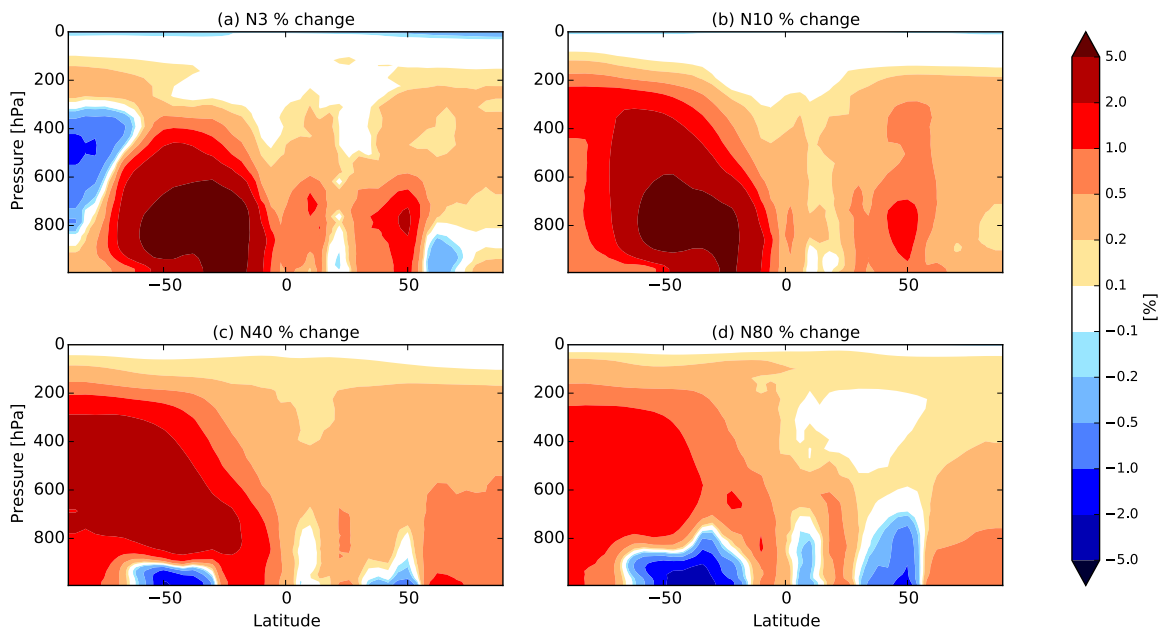
1
 2 Figure 2. Mean millennial fixed yield biogenic SOA formation from (a) MEGAN emissions and
 3 (b) LPJ-GUESS emissions between the periods 1000-2000 in $\text{mg m}^{-2} \text{day}^{-1}$. Absolute change in
 4 fixed yield biogenic SOA formation from averaged (c) MEGAN BVOC emissions (monoterpenes,
 5 isoprene and sesquiterpenes) and (d) LPJ-GUESS BVOC emissions (monoterpenes and
 6 isoprene) between 1000 and 2000 in $\text{mg m}^{-2} \text{day}^{-1}$. Relative change in fixed yield biogenic SOA
 7 formation from averaged (e) MEGAN BVOC emissions (monoterpenes, isoprene and
 8 sesquiterpenes) and (f) LPJ-GUESS BVOC emissions (monoterpenes and isoprene) between
 9 1000 and 2000. An increase in SOA formation in (c), (d), (e) and (f) is represented by red
 10 colors, and a decrease in SOA formation by blue.



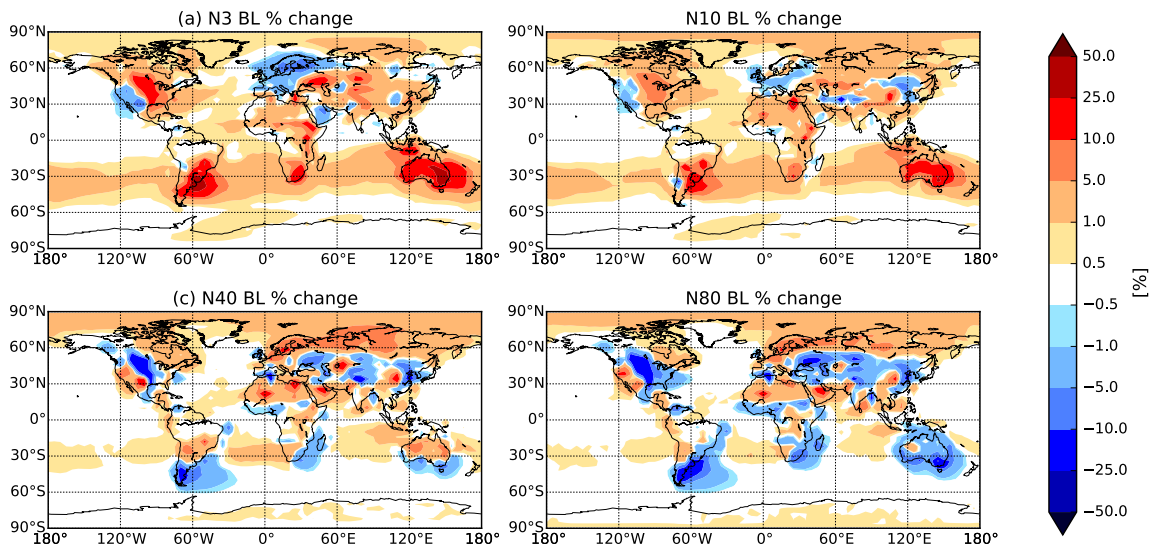
1
 2 Figure 3. Percent contribution to SOA formation by (a) isoprene, (b) monoterpene and (c)
 3 sesquiterpene emissions from the MEGAN reconstruction, averaged over the years 1000-2000.
 4 The area enclosed by the red contour represents greater than 5% of the maximum mean
 5 millennial SOA formation from emissions of BVOCs (isoprene + monoterpenes +
 6 sesquiterpenes).



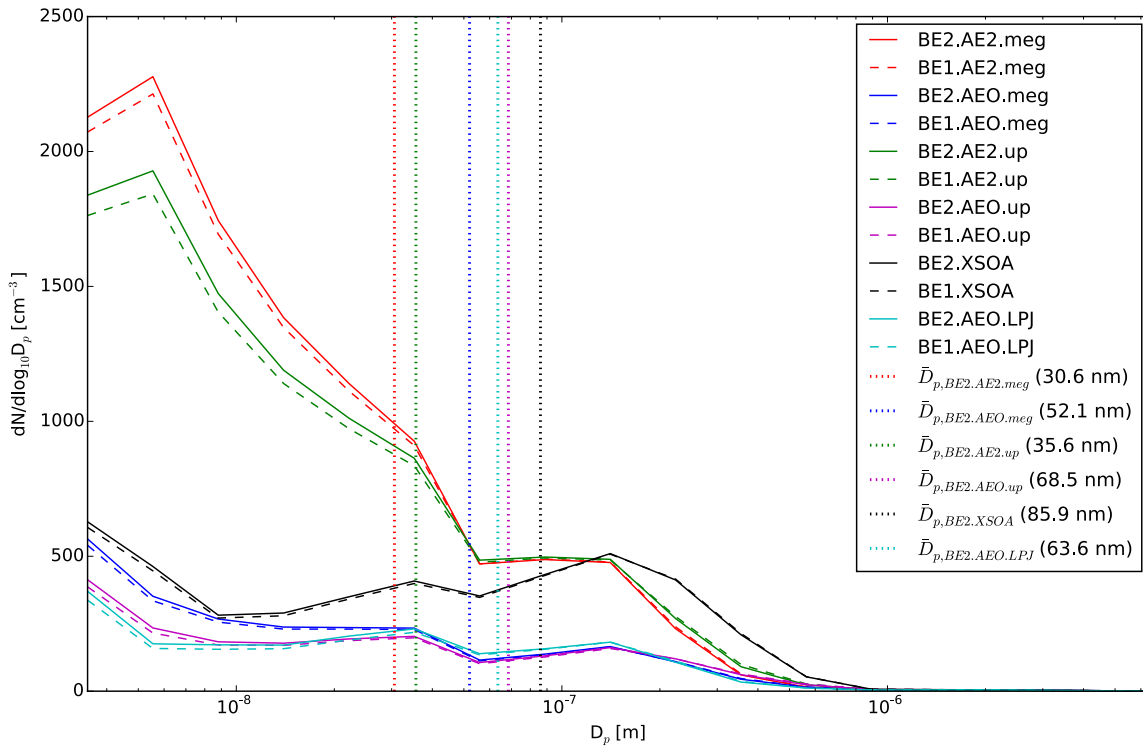
1
 2 Figure 4. Percentage change in annually averaged boundary layer (a) N3, (b) N10, (c) N40 and
 3 (d) N80 (number of particles with diameter greater than 3 nm, 10 nm, 40 nm and 80 nm
 4 respectively) when changing MEGAN BVOC emissions from year 1000 to year 2000 with
 5 constant present day anthropogenic emissions (2005) (BE2.AE2.meg – BE1.AE2.meg).
 6 Globally averaged, N3 and N10 increased by 2.3% and 1.5% respectively, whereas N40 and
 7 N80 decreased by 0.6% and 1.3% respectively (see Table 2). An increase in particle number
 8 concentration is represented by red colors, and a decrease in blue.



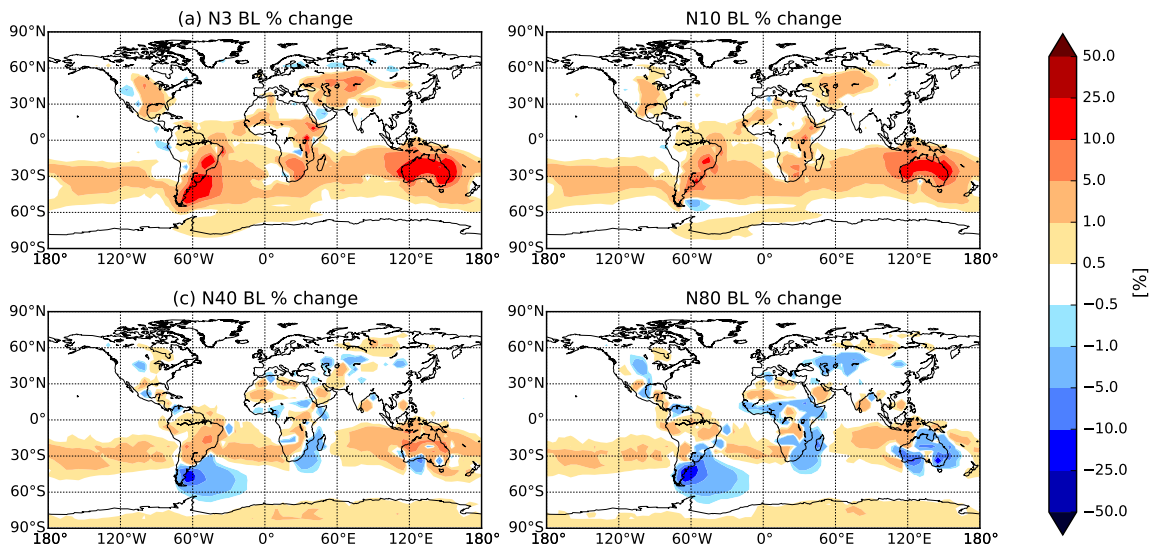
1
 2 Figure 5. Zonal-mean annual-average percentage change in (a) N3, (b) N10, (c) N40 and (d)
 3 N80 when changing MEGAN BVOC emissions from year 1000 to year 2000 with constant
 4 present day anthropogenic emissions (2005) (BE2.AE2.meg – BE1.AE2.meg). An increase in
 5 particle number concentration is represented by red colors, and a decrease in blue.



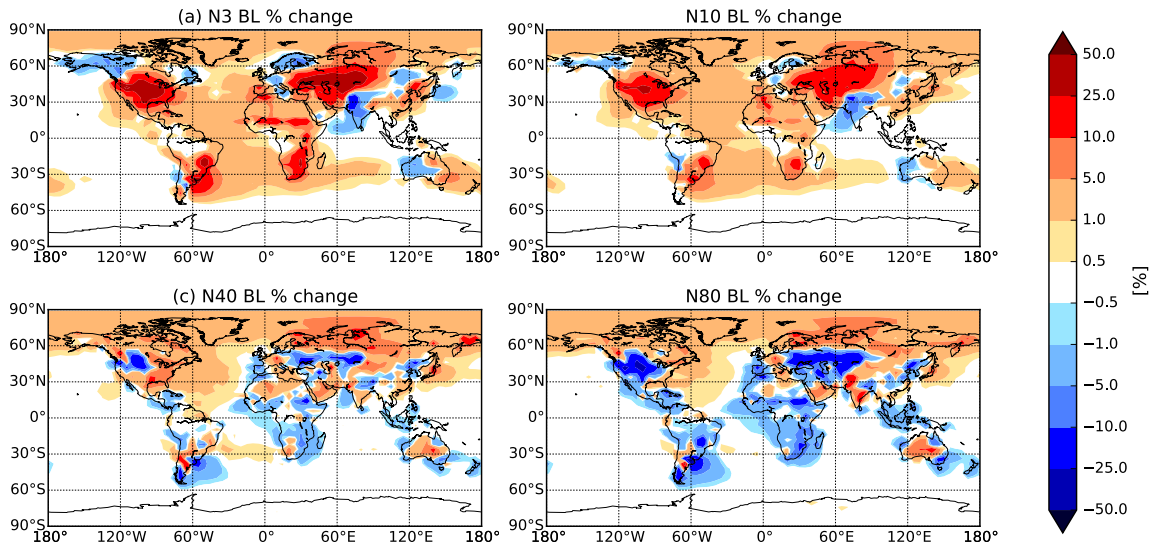
1
 2 Figure 6. Percentage change in annually averaged boundary layer (a) N3, (b) N10, (c) N40 and
 3 (d) N80 when changing MEGAN BVOC emissions from year 1000 to year 2000 with
 4 anthropogenic emissions off (BE2.AEO.meg – BE1.AEO.meg). Globally averaged, N3, N10
 5 and N40 increased by 3.2%, 1.9% and 0.4% respectively, whereas N80 decreased by 0.6%
 6 (see Table 2). An increase in particle number concentration is represented by red colors, and a
 7 decrease in blue.



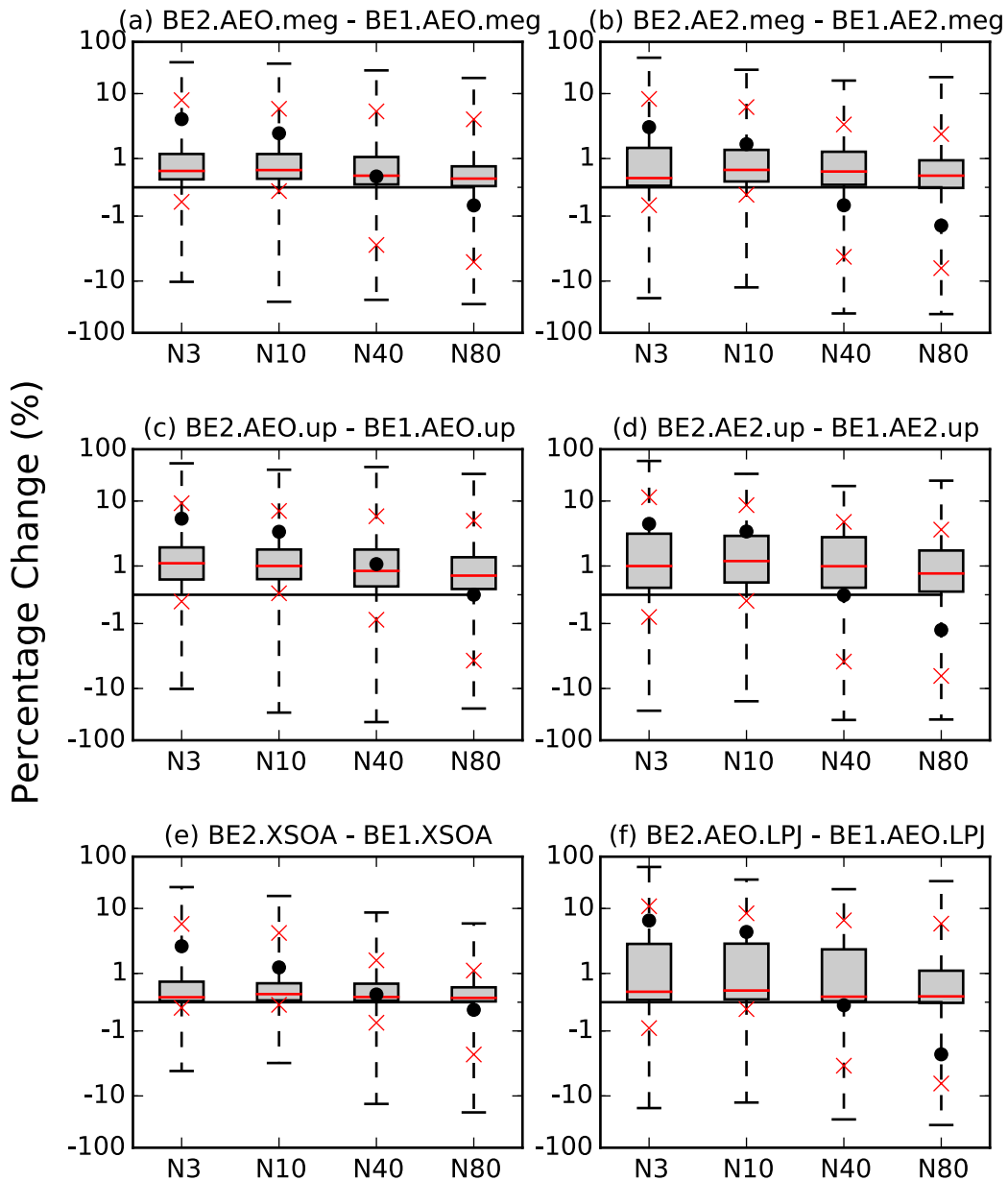
1
 2 Figure 7. Simulated global boundary layer annual-mean particle number size distributions for
 3 the simulations outlined in Table 1. The vertical dotted lines represent the mean diameter for the
 4 simulations using year 2000 biogenic emissions (BE2.AE2.meg, BE2.AEO.meg, BE2.AE2.up,
 5 BE2.AEO.up, BE2.XSOA and BE2.AEO.LPJ).



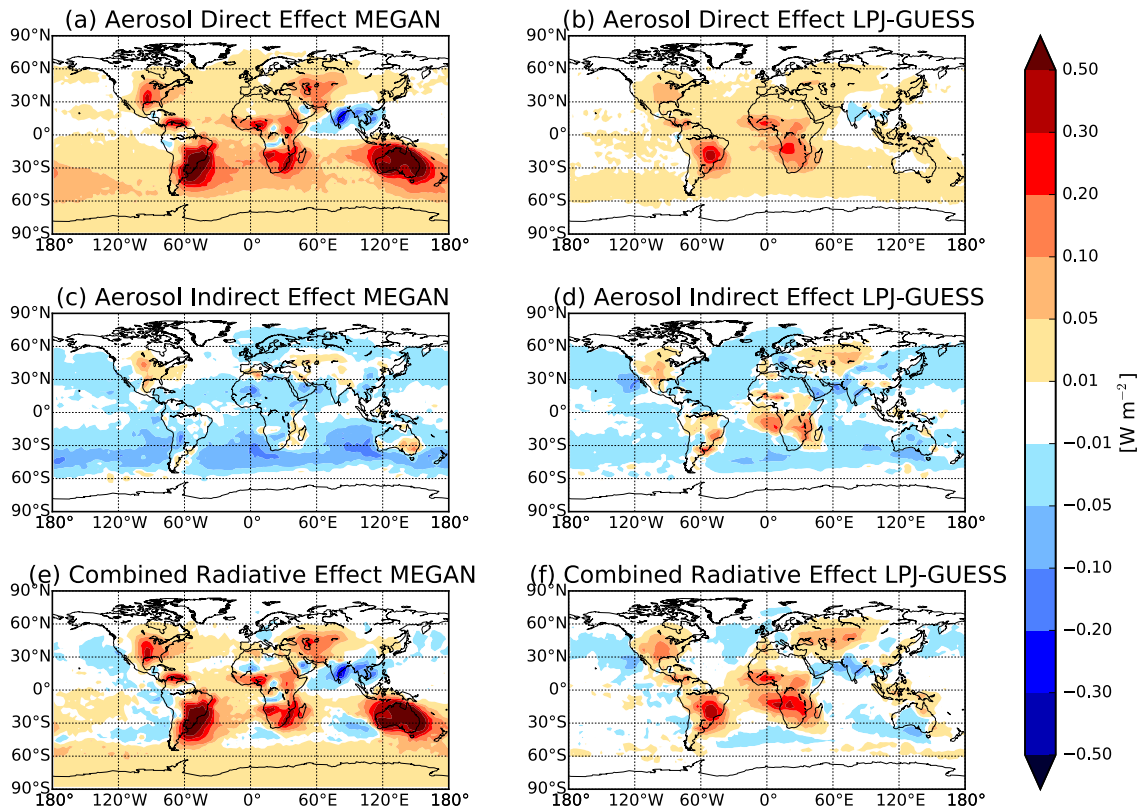
1
 2 Figure 8. Percentage change in annually averaged boundary layer (a) N3, (b) N10, (c) N40 and
 3 (d) N80 when changing MEGAN BVOC emissions from year 1000 to year 2000 with constant
 4 present day anthropogenic emissions (2005) including an additional 100 Tg (SOA) yr⁻¹ as per
 5 D'Andrea et al. (2013) (BE2.XSOA – BE1.XSOA). Globally averaged, N3, N10 and N40
 6 increased by 1.9%, 1.2% and 0.3% respectively, whereas N80 decreased by 0.3% (see Table
 7 2). An increase in particle number concentration is represented by red colors, and a decrease
 8 in blue.



1
 2 Figure 9. Percentage change in annually averaged boundary layer (a) N3, (b) N10, (c) N40 and
 3 (d) N80 when changing LPJ-GUESS BVOC emissions from year 1000 to year 2000 with
 4 anthropogenic emissions off (BE2.AEO.LPJ – BE1.AEO.LPJ). Globally averaged, N3 and N10
 5 increased by 5.9% and 3.5% respectively, whereas N40 and N80 decreased by 0.1% and 1.8%
 6 respectively (see Table 2). An increase in particle number concentration is represented by red
 7 colors, and a decrease in blue.



1
 2 Figure 10. Global percent changes in N3, N10, N40 and N80 for biogenic emissions from 1000
 3 to 2000 on a logarithmic scale for the simulations (a) BE2.AEO.meg – BE1.AEO.meg, (b)
 4 BE2.AE2.meg – BE1.AE2.meg, (c) BE2.AEO.up – BE1.AEO.up, (d) BE2.AE2.up – BE1.AE2.up,
 5 (e) BE2.XSOA – BE1.XSOA, and (f) BE2.AEO.LPJ – BE1.AEO.LPJ. The black dots indicate
 6 the global mean, the red line is the global median, the grey boxes are the interquartile range,
 7 the whiskers are the global maximum and minimum changes and the red X's indicate the 5th
 8 and 95th percentiles (see Table 2).



1
 2 Figure 11. Annual mean change between year 1000 and year 2000 in (a) DRE with MEGAN
 3 BVOC emissions and anthropogenic emissions off (BE2.AEO.meg – BE1.AEO.meg), (b) DRE
 4 with LPJ-GUESS BVOC emissions and anthropogenic emissions off (BE2.AEO.LPJ –
 5 BE1.AEO.LPJ), (c) AIE with MEGAN BVOC emissions and anthropogenic emissions off, (d) AIE
 6 with LPJ-GUESS BVOC emissions and anthropogenic emissions off, (e) combined radiative
 7 effect with MEGAN BVOC emissions and anthropogenic emissions off, and (f) combined
 8 radiative effect with LPJ-GUESS BVOC emissions and anthropogenic emissions off. Global
 9 mean changes are $+0.065 \text{ W m}^{-2}$, $+0.022 \text{ W m}^{-2}$, -0.020 W m^{-2} , -0.008 W m^{-2} , $+0.049 \text{ W m}^{-2}$, and
 10 $+0.015 \text{ W m}^{-2}$ respectively (see Table 3).